



**I
N
A
O
E**

Control in quantum optomechanical systems

by

Christian Ventura Velázquez
M.Sc., INAOE

Dissertation
submitted to the Program in Optics, Department of Optics,
in partial fulfillment of requirements for the degree of

Doctor in Science with speciality in Optics

at the

Instituto Nacional de Astrofísica, Óptica y Electrónica
August 2019
Tonantzintla, Puebla

Advisors:

Dr. Blas Manuel Rodríguez Lara,
Investigador titular, INAOE
Dr. Benjamín Raziel Jaramillo Ávila
Cátedra CONACyT, INAOE

©INAOE, 2019

All rights reserved

The author hereby grants to INAOE permission to reproduce and
to distribute copies of this thesis document in whole or in part.



*Para mi madre,
con mi amor y gratitud.
Mi mayor ejemplo y apoyo.*

Resumen

Los sistemas optomecánicos son poderosos dispositivos tanto para responder preguntas fundamentales en la física cuántica o como para aplicaciones tecnológicas. Con éstos podríamos llegar a observar la transición entre la física clásica y la cuántica, o fenómenos puramente cuánticos con objetos a escala mesoscópica. Por el lado de fundamentos, ha sido posible obtener comportamientos cuánticos en objetos mesoscópicos, como el estado base cuántico del oscilador mecánico. Sobre aplicaciones tecnológicas, los sistemas optomecánicos pueden ser incorporados en chip para diferentes usos, como circuladores o aisladores que no necesitan campos magnéticos para funcionar. En los últimos ejemplos, la fase del láser es usada como parámetro de control para producir el efecto deseado en arreglos optomecánicos. Entonces, es relevante estudiar los sistemas optomecánicos y la forma de controlarlos para obtener muchos más comportamientos interesantes y aplicaciones.

En esta tesis se trabaja con sistemas optomecánicos bombeados. Éstos dispositivos consisten de un oscilador mecánico acoplado a un campo electromagnético por medio de fuerzas causadas por presión de radiación. Los resultados presentan dos técnicas para controlar la dinámica abierta del sistema optomecánico. La primera técnica produce robustez en la transferencia de estados cuánticos entre el modo mecánico y el electromagnético. La segunda se centra en regímenes optomecánicos efectivos de la simetría \mathcal{PT} . Ambas técnicas emplean las características del láser. La primera se basa en modular de la fase del láser y la segunda en valores de la potencia. Los enfoques para estudiar la dinámica abierta del sistema emplean ecuaciones cuánticas de Langevin y la ecuación maestra de Lindblad. Dada la naturaleza abierta del sistema, parte del análisis es analítico mientras que otros resultados fueron obtenidos con simulaciones numéricas.

Esquema de la tesis

El Capítulo 1 introduce la interacción optomecánica y sus realizaciones experimentales. También se da una descripción del modelo cuántico de los sistemas optomecánicos y sus regímenes linealizados. Adicionalmente, una tabla presenta parámetros optomecánicos relevantes que han sido publicados en revistas internacionales. Este capítulo se ocupa de introducir el conocimiento básico sobre los sistemas optomecánicos.

El Capítulo 2 presenta el marco teórico usado en el estudio de las técnicas de control. Tres son los temas descritos: el primero es sobre los dos enfoques usados para el estudio de sistemas cuánticos abiertos, y los otros dos están directamente relacionados con las dos técnicas propuestas para el control de sistemas optomecánicos abiertos.

Finalmente, los Capítulos 3 y 4 muestran los resultados analíticos y numéricos obtenidos para las técnicas de control propuestas en el sistema optomecánico bombeado con un láser.

Abstract

Optomechanical systems are powerful devices both as experiments to answer fundamental questions related with quantum physics as for technological applications. They will enable us to observe the transition between classical and quantum physics, or purely quantum phenomena with objects at mesoscopic scale. As an example on the fundamental side, it is possible to obtain quantum behaviours of mesoscopic objects, like the quantum ground state of the mechanical oscillator. Regarding technological applications, optomechanical systems can be incorporated on-chip for different uses, like magnetic-free circulators or isolators. In the latter example, the laser's phase is used as control parameter to produce a desired effect on optomechanical arrangements. Then, it is relevant to study optomechanical systems and the way those can be controlled in order to obtain many other interesting behaviours and applications.

This thesis deals with driven optomechanical systems. These devices consist of one mechanical oscillator coupled to an electromagnetic field by radiation pressure forces. The results present two techniques to control the optomechanical open dynamics. The first technique produces robust quantum-state transfer between the mechanical and electromagnetic fields. The second is focused in effective optomechanical \mathcal{PT} -symmetry regimes. Both techniques use characteristics of the laser. The first one relies on phase modulation of the laser while the second on its power value. The approaches to study the optomechanical open dynamics are based on quantum Langevin equations and master equation in Lindblad form. Because the system is open, part of the analysis is analytical while other results were obtained with numerical simulations.

Thesis outline

Chapter 1 introduces the optomechanical interaction and its experimental realization. It also describes the quantum model of optomechanical systems and its linearized regimes. These are used throughout the thesis. Additionally, a table summarizes relevant optomechanical parameters reported in international publications. This chapter serves as introduction to the basic knowledge about optomechanical systems.

Chapter 2 presents the theoretical framework used to study the control techniques proposed for interesting quantum behaviour of the optomechanical systems. The topics covered are three: the first is related with two approaches to study open quantum systems, and the last two topics are directly concerned with the two control techniques proposed for the open optomechanical system.

Finally, Chapters 3 and 4 show the analytical and numerical results obtained for the two techniques proposed to control the optomechanical systems driven by a laser.

Acknowledgements

Through these four years, in which I developed this project, I acquired lots of experiences and friends. Many people have been made possible the success of this thesis. Here, I want to pay a humble recognition to all of them.

First, I thank my advisors Dr. Blas and Dr. Benjamín. Their teachings were the fundamental guide for my research project. They supported my ideas and made them come out in a way scientists must do it and that is the main teaching they could give me. We know it was not easy, through this project I failed many times and they continued encouraging me to do my best, **THANKS !** I hope both of you really know how grateful I am.

Danke Prof. Dr. Peter Rabl who hosted me in his group for Quantum Optics Theory at TU Wien, Vienna. There, I felt welcomed and I interacted with so many nice people. I could open my view to other interesting research fields and that is invaluable.

I would like to thank the CONACyT for the two scholarships given to me during these four years. That financial fund was primordial for my project and allowed me to acquire much more scientific skills. Also, thanks to INAOE for the facilities, funds and nice preserved environment.

I want to thank many other people. Among them are my colleagues at the group of Quantum Optics at INAOE. Their friendship made the daily life at office more enjoyable. Last but not least, my mother and pets, my beloved family who are the ones I find support.

*The God whom science recognizes must be a
God of universal laws exclusively, a God
whom does a wholesale, not a retail business.
He cannot accommodate his processes to the
convenience of individual.*

- WILLIAM JAMES -

Contents

1	The Optomechanical Interaction	1
1.1	Introduction	1
1.1.1	Experimental realizations	2
1.2	Quantum model	2
1.2.1	Linearized approach	3
2	Theoretical framework	7
2.1	Quantum Langevin equations	7
2.1.1	Markov Approximation	8
2.1.2	Linearized optomechanical system	10
2.2	Master Equation	12
2.2.1	Born and Markov approximations	13
2.3	Composite pulse sequence for a qubit	15
2.4	\mathcal{PT} -symmetry	17
2.4.1	Gain-loss system	18
3	Robust quantum-state transfer	21
3.1	Quantum excitation exchange	21
3.2	Phase-sequence for a robust quantum excitation exchange	23
3.2.1	Angular momentum representation and statistical analysis	26
3.2.2	Longer composite sequences	28
3.3	Smooth phase-sequence	29
3.4	Conclusions	31
4	Non-Hermitian optomechanics	33
4.1	Optomechanical eigenfrequencies	33
4.1.1	\mathcal{PT} -symmetry approach	34
4.2	Differences in the evolutions	35
4.2.1	Numerical simulations	37
4.3	Conclusions	39
5	Conclusions	41
A	Publications derived from the research presented in this thesis	43

Chapter 1

The Optomechanical Interaction

This chapter presents a review of optomechanical systems. We go from the first experimental observations of mechanical vibrations in a cavity due to an electromagnetic (EM) field, to many other effects in a large variety of devices. All of these effects are caused by the non-linear coupling between the EM field and the mechanical vibration [1]. Classical EM theory can explain some effects, while for some others it is necessary to introduce quantum fluctuations. With the latter, we obtain a linear interaction in which two main behaviours are well-known: the blue- and red- sidebands. In the end, optomechanical systems are a promising candidate to observe quantum signatures of macroscopic objects.

1.1 Introduction

The optomechanical interaction relies on the coupling between mechanical oscillations and an EM field [2]. This phenomena is originated by the light's momentum which gives rise to radiation pressure forces [3]. Maxwell predicted this effect [4] and it was confirmed few decades ahead [5–8]. The radiation pressure depends on the EM field's intensity and at the quantum level it depends on the number of photons. We can separate them in two categories: gradient forces and scattering forces. The first category, also known as dipole force, forms the basis of optical tweezers set-ups [9] and it is caused by nonzero space variations in the EM field [10–12]. The second category, scattering forces, are consequence of the momentum transfer from the EM field to an object. This is the mechanism through which the optomechanical interaction was obtained. Although, it is also possible to obtain optomechanical coupling with gradient forces [13, 14]. Interestingly, the optomechanical interaction couples two oscillatory systems which have very different characteristic frequencies, Table 1.1.

The first works related to optomechanical phenomena date back to interferometric studies on gravitational waves [15–19]. These studies considered radiation pressure effects on large-scale Fabry-Pérot cavities. Their analysis revealed limits on the interferometer's sensitivity due to quantum nature of light and the possibility of cooling or heating the mechanical vibrations. In later experiments, optical bistability was observed in optomechanical cavities [20, 21] and explained with classical EM theory [22, 23]. Those optomechanical cavities consisted of an optical or microwave cavity that contains a mechanical element, one lightweight mirror free to oscillate, with an incident EM field which can be tuned in power and frequency. They showed

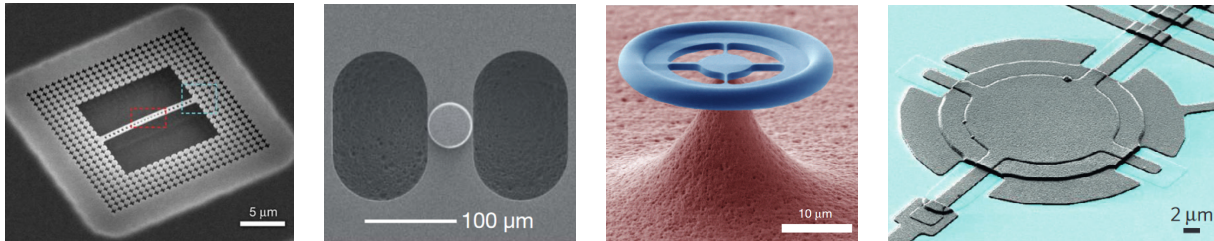


Figure 1.1: Four examples of the mechanical element in optomechanical systems. From left to right: a patterned silicon nanobeam from Ref. [69], a high-reflectivity mirror pad of a Fabry-Pérot cavity from Ref. [75], a spoke-anchored toroidal resonator from Ref. [86], and a mechanically compliant vacuum-gap capacitor from Ref. [79].

hysteresis effects characteristic of bistable response on the output power measured. This is consequence of the radiation pressure exerted on the mechanical element. A more recent work studied the range of frequency and amplitude values of the driving where the bistability behaviour can be observed even at the level of quantum fluctuations [24]. Theoretical proposals of quantum optics due to optomechanical interactions have been originated since then: generation of squeezed light [25,26], quantum non-demolition measurements [27,28], optomechanical cooling [29], entanglement [30–32], quantum-state transfer [33], non-reciprocal response [34], photon blockade [35], topologically protected phonon transport [36], and some others [37–44].

1.1.1 Experimental realizations

Advances in material science and nanofabrication techniques enable the exploration of optomechanical interactions in a variety of devices, like microtoroid resonators [45–47], micromirrors [48, 49], membranes [50, 51], microdisks [52, 53], microspheres [54–56], photonic crystals [57, 58], nanobeams [59, 60], superconducting circuits [61], and levitated nanoparticles [62]. Generically, we refer to these as optomechanical systems. Another experimental set-ups like atomic clouds [63, 64] and fluids [65–68] can work as optomechanical systems. This wide variety of devices has made possible the experimental realization for some of the previously mentioned proposals. One example is the cooling of the mechanical element to its quantum ground state [69–71]. Other experiments showed optomechanically induced transparency [72–74], optomechanical normal-mode splitting [70, 75], entanglement [76–78], observation of the mechanical quantum vacuum fluctuations [79], mechanical squeezing [80], non-reciprocal behaviour [81, 82], non-classical mechanical states [83, 84], and Bell test for the quantum behaviour of the mechanical element [85].

1.2 Quantum model

Some decades ago, theoretical works about the effects of the radiation pressure in the interferometers to detect gravitational waves gave as results the quantum model for the optomechanical interaction. The model describes a Fabry-Pérot cavity with resonance frequency ω_c . This cavity posses one mirror which partially reflects light and the other is totally reflecting.

The latter oscillates at frequency ω_m due to the pressure exerted by the light circulating inside the cavity. The non-linear optomechanical interaction for this system is described by the Hamiltonian [87, 88], with $\hbar = 1$,

$$\hat{H}_{OM} = \omega_c \hat{a}^\dagger \hat{a} + \omega_m \hat{b}^\dagger \hat{b} + g_0 \hat{a}^\dagger \hat{a} (\hat{b}^\dagger + \hat{b}), \quad (1.1)$$

where the cavity (mechanical) mode has an annihilation operator \hat{a} (\hat{b}) and the optomechanical coupling strength is g_0 . Even though this Hamiltonian was derived for optomechanical cavities, the devices mentioned in Sec. 1.1.1 also fit in this quantum model. Interestingly, the coupling g_0 depends on the geometry of every device, for a Fabry-Pérot cavity of length L , g_0 is proportional to L^{-1} , while for a microtoroid of radio R , g_0 is proportional to R^2 [2]. Additionally, in some devices it is possible to couple the EM field with the square of the mechanical displacement, $\hat{a}^\dagger \hat{a} (\hat{b}^\dagger + \hat{b})^2$ [50, 89, 90]. Such quadratic coupling has been proposed as candidate to observe individual quantum jumps of the phonons [91]. More generally, due to the oscillations of the mechanical element, the frequency of the cavity is modulated in a way that $\omega_c(x) = \omega_c + (\partial_x \omega_c) x + (\partial_x^2 \omega_c) x^2 + \dots$. From this, we can appreciate the standard coupling showed in Eq. (1.1) and the quadratic one, $\propto x^2$.

1.2.1 Linearized approach

Here we review the linearization of the optomechanical interaction. This approach is based on Ref. [23, 25–27]. Those authors considered a classical component plus a quantum fluctuation for the cavity and mechanical operators,

$$\hat{a} \rightarrow \alpha + \hat{c}, \quad (1.2a)$$

$$\hat{b} \rightarrow \beta + \hat{d}. \quad (1.2b)$$

This linearization is also obtained using a displacement operator $\hat{D}_z(\varsigma) = \exp(\varsigma \hat{z}^\dagger + \varsigma^* \hat{z})$, which acts as $\hat{D}_z^\dagger(\varsigma) \hat{z} \hat{D}_z(\varsigma) = \hat{z} + \varsigma$. The classical component is seen as a semiclassical field amplitude, *i. e.*, we have $\alpha = \langle \hat{a} \rangle$ and $\beta = \langle \hat{b} \rangle$. In consequence the mean number of photons injected by the laser is $|\alpha|^2 = n_p$.

In experiments the optomechanical system is driven by a strong laser with frequency ω_p . Then, we can write the Hamiltonian with the pumping like, with $\hbar = 1$,

$$\hat{H} = \hat{H}_{OM} + i\varepsilon \cos(\omega_p t + \phi) (\hat{a}^\dagger - \hat{a}), \quad (1.3)$$

where ϕ is a constant phase and ε is the strength of the laser. We move to the frame rotating at the laser frequency, so we can write the Hamiltonian (1.3) as,

$$\hat{H}_0 = (\omega_c - \omega_p) \hat{a}^\dagger \hat{a} + \omega_m \hat{b}^\dagger \hat{b} + g_0 \hat{a}^\dagger \hat{a} (\hat{b}^\dagger + \hat{b}) + i \frac{\varepsilon}{2} (e^{i\phi} \hat{a}^\dagger - e^{-i\phi} \hat{a}). \quad (1.4)$$

In this Hamiltonian we used the rotating wave approximation (RWA), *i. e.*, we neglect those terms rotating at high frequency [92] in the part correspondent to the driving. Now, we use Eq.(1.2) in this last Hamiltonian. As result we obtain four contributions: one which just

contains scalars and it is omitted, the second is only proportional to the quantum fluctuation operators and from which we found the expressions for α and β , the third is a non-linear term, $\propto \hat{c}^\dagger \hat{c} (\hat{b}^\dagger + \hat{b})$, and the fourth is the linearized Hamiltonian,

$$\hat{H}_{lin} = -\Delta \hat{c}^\dagger \hat{c} + \omega_m \hat{d}^\dagger \hat{d} + g \left(e^{i\phi'} \hat{c}^\dagger + e^{-i\phi'} \hat{c} \right) \left(\hat{d}^\dagger + \hat{d} \right), \quad (1.5)$$

where we define a detuning $\Delta = \omega_p - \omega_c - 2g_0 \text{Re}(\beta)$, the enhanced optomechanical coupling $g = g_0 |\alpha| = g_0 \sqrt{n_p}$ and the phase $\phi' = \arg(\alpha)$. Here, we see a shift in the detuning caused by optomechanical coupling and the semiclassical field amplitude of the mechanical oscillations.

The expressions obtained for the mean field amplitudes are,

$$\alpha = -\frac{i e^{-i\phi} \varepsilon}{2\Delta}, \quad (1.6a)$$

$$\beta = -\frac{g_0 |\alpha|^2}{\omega_m}. \quad (1.6b)$$

Up to this point, we have not taken into account any loss of the system, in Sec. 2.1.2 will do it. From these expressions, we already can see the bistable behaviour of the output EM field [20, 21]. This is caused by the dependence of semiclassical EM field amplitude, α , on the number of photons injected by the laser, $|\alpha|^2 = n_p$. Interestingly, the enhanced optomechanical coupling gets stronger as the laser strength increases. From this property we can neglect the non-linear term which results in the process to linearise the Hamiltonian \hat{H}_0 . Its contribution is smaller compared with the one of \hat{H}_{lin} .

From the linearized Hamiltonian, Eq. (1.5), we move to the frame rotating with the Hamiltonian $-\Delta \hat{c}^\dagger \hat{c} + \omega_m \hat{d}^\dagger \hat{d}$ to obtain the interaction terms,

$$e^{i\phi' + i(\omega_m - \Delta)t} \hat{c}^\dagger \hat{d}^\dagger + e^{-i\phi' - i(\omega_m - \Delta)t} \hat{c} \hat{d} + e^{i\phi' - i(\omega_m + \Delta)t} \hat{c}^\dagger \hat{d} + e^{-i\phi' + i(\omega_m + \Delta)t} \hat{c} \hat{d}^\dagger. \quad (1.7)$$

This form allows us to apply a RWA depending on the value of the detuning Δ . We have the so-called red- and blue- detuning regimes for $\Delta = -\omega_m$ and $\Delta = +\omega_m$, respectively. Even though this analysis is semiclassical, similar sidebands are found in the purely quantum [35, 93, 94] or classical regimes [95].

We focus on the two regimes mentioned before because the interaction can be reduced with the RWA into a two well-know quantum cases:

Red-detuned regime where $\Delta = -\omega_m$. With the RWA, we just consider the interaction terms,

$$e^{i\phi'} \hat{c}^\dagger \hat{d} + e^{-i\phi'} \hat{c} \hat{d}^\dagger, \quad (1.8)$$

which corresponds to a beam-splitter-like interaction [96]. This interaction allow the quantum-state transfer between the EM and mechanical fields. Alternatively, we can use it to cool the mechanical motion [1, 79].

Blue-detuned regime where $\Delta = +\omega_m$. With the RWA, we just consider the interaction terms,

$$e^{i\phi'} \hat{c}^\dagger \hat{d}^\dagger + e^{-i\phi'} \hat{c} \hat{d}, \quad (1.9)$$

Ref.	Structure	$\omega_c/2\pi$ [Hz]	$\kappa/2\pi$ [Hz]	$\omega_m/2\pi$ [Hz]	$\gamma/2\pi$ [Hz]	$g_0/2\pi$ [Hz]	T [K]
[75]	FP	1.77 P	215 k	947 k	140	2.7	< 300 m
[90]	NR	7.5 G	600 k	6.3 M	≈ 6.3	84 k	100 m
[70]	VGC	7.54 G	200 k	10.56 M	32	200.9	25 m
[86]	TMC	30.78 T	6.04 M	78.226 M	2.2 M	3.4 k	650 m
[76]	VGC	7.72 G	660 k	10.34 M	35	200	< 20 m
[79]	VGC	10.188 G	163 k	15.9 M	150	300	25 m
[97]	PNB	30.78 T	817 M	5.6 G	3 M	645 k	rT
[98]	FP	1.77 P [75]	1.3 M	914 k	4.25 k	40 k	rT
[99]	NB	47.714 P	550 M	4.5 M	15	50 k	rT
[84]	PNB	30.69 T	846 M	5.25 G	13.82 k	869 M	35 m
[67]	SF	194.5 T	46.1 M	317.5 M	$\gamma(T)$	3.3 k	< 0.5
[61]	SCC	5.4 G	1.2 M	583.5 G	300 k	15 k	1.8

Table 1.1: Optomechanical parameters obtained from published experimental realizations. Here, the photons (phonons) frequency is ω_c (ω_m) with decay rate κ (γ), the optomechanical coupling strength is g_0 and the temperature of the bath is T . The mechanical element is designed with the letters: FP for a micromirror of a Fabry-Pérot cavity, NR for nanomechanical resonator, VGC for vacuum-gap capacitor, TMC for toroidal microcavity, PNB for patterned silicon nanobeam, NB for nanomechanical beam, SF for superfluid Helium, SCC for superconducting circuit. Additionally, we use the symbols for the prefixes of the International System of Units and $rT = 293K$ stands for room temperature.

which corresponds to a non-degenerate parametric amplifier [92]. This interaction is used for the generation of pairs photon-phonon or the exponential growth of energy of the EM field and the mechanical motion [1, 79].

Some experiments play with these two regimes in order to obtain different quantum behaviours, like read out of entangled states [76, 77], measurement of the mechanical vacuum fluctuations [79], and non-classical correlations [83, 84].

Chapter 2

Theoretical framework

This chapter introduces the tools we used to analyse the lossy dynamics of optomechanical systems. First, we discuss two approaches to study time evolution for the system of interest: the quantum Langevin equations (QLEs) and the master equation in Lindblad form. Both approaches are useful to study quantum open systems, the QLEs work with the system's operators and the master equation uses the system's density operator. Second, we review how phase-driving produces robustness in the population transfer of a qubit without considering losses [100–103]. This technique was implemented successfully to overcome the systematic errors of some parameters related to the coherent driving, like the field amplitude, pulse duration or detuning [104]. Finally, we briefly review the \mathcal{PT} -symmetry topic with an specific emphasis on a photonic gain-loss system.

2.1 Quantum Langevin equations

In experiments, is impossible to completely isolate our system of interest from the environment, which is considered as a set of secondary degrees of freedom. That coupling between our system and the environment leads to a dynamics which is usually quite hard to solve exactly. We derive effective equations for the dynamics of the open system. This allows us to study its time evolution in a more tractable way, while taking into account the effects due to the environment [105, 106].

To intuitively derive the QLEs, we proceed to obtain those for an unspecified system interacting with the environment which is modeled as a continuum of harmonic oscillators. The Hamiltonian for our purpose is composed of three parts, the system of interest, \hat{H}_S ; the environment, \hat{H}_B ; and the interaction between both, \hat{H}_I . Our system has a characteristic frequency ω_0 which is the largest of the parameters and justifies a RWA that we use to write the interaction part \hat{H}_I . The Hamiltonians for the environment, also called bath, \hat{H}_B , and for the interaction, \hat{H}_I , with $\hbar = 1$,

$$\hat{H}_B = \int \omega \hat{b}^\dagger(\omega) \hat{b}(\omega) d\omega, \quad (2.1a)$$

$$\hat{H}_I = i \int \lambda(\omega) \left[\hat{b}^\dagger(\omega) \hat{c} - \hat{c}^\dagger \hat{b}(\omega) \right] d\omega. \quad (2.1b)$$

Here, the bath has a bosonic operator $\hat{b}(\omega)$ obeying $[\hat{b}(\omega), \hat{b}^\dagger(\tilde{\omega})] = \delta(\omega - \tilde{\omega})$ and \hat{c}_S is the system's operator which describes how it couples to the bath.

The Heisenberg equations of motion for an arbitrary system operator, \hat{O}_S , are obtained using the complete Hamiltonian $\hat{H} = \hat{H}_S + \hat{H}_B + \hat{H}_I$. Then,

$$\frac{d\hat{O}_S}{dt} = i [\hat{H}, \hat{O}_S] \quad (2.2a)$$

$$= i [\hat{H}_S, \hat{O}_S] - \int \lambda(\omega) \left\{ \hat{b}^\dagger(\omega) [\hat{c}_S, \hat{O}_S] - [\hat{c}_S^\dagger, \hat{O}_S] \hat{b}(\omega) \right\} d\omega. \quad (2.2b)$$

The bath operators obey the Heisenberg equation,

$$\frac{d\hat{b}(\omega)}{dt} = i [\hat{H}, \hat{b}(\omega)], \quad (2.3a)$$

$$= -i\omega \hat{b}(\omega) - \int \lambda(\omega') [\hat{b}^\dagger(\omega'), \hat{b}(\omega)] \hat{c}_S d\omega', \quad (2.3b)$$

$$= -i\omega \hat{b}(\omega) + \lambda(\omega) \hat{c}_S. \quad (2.3c)$$

By integrating Eq. (2.3), we obtain,

$$\hat{b}(\omega, t) = e^{-i\omega t} \hat{b}(\omega, 0) + \lambda(\omega) \int^t \hat{c}_S(s) e^{-i\omega(t-s)} ds. \quad (2.4)$$

We substitute this result in Heisenberg's equation, Eq. (2.2), which yields,

$$\begin{aligned} \frac{d\hat{O}_S}{dt} &= i [\hat{H}_S, \hat{O}_S] - \int d\omega \lambda(\omega) \left\{ e^{i\omega t} \hat{b}^\dagger(\omega, 0) [\hat{c}_S, \hat{O}_S] - [\hat{c}_S^\dagger, \hat{O}_S] e^{-i\omega t} \hat{b}(\omega, 0) \right\} \\ &\quad - \int d\omega \lambda^2(\omega) \int^t ds \left\{ e^{i\omega(t-s)} \hat{c}_S^\dagger(s) [\hat{c}_S, \hat{O}_S] - [\hat{c}_S^\dagger, \hat{O}_S] e^{-i\omega(t-s)} \hat{c}_S(s) \right\}. \end{aligned} \quad (2.5)$$

2.1.1 Markov Approximation

We use the next assumption: the coupling is valid within a bandwidth $2\Delta_B \ll \omega_0$ around ω_0 , *i. e.*, in the interval $\Omega = (\omega_0 - \Delta_B, \omega_0 + \Delta_B)$. In that frequency range, the coupling strength may be approximated by a constant value, λ . This assumption allows us to simplify Eq. (2.5). Taking into account the assumption for the coupling strength, we define the input field of the bath as,

$$\hat{b}_{in}(t) := \frac{1}{\sqrt{2\pi}} \int_{\Omega} e^{-i\omega t} \hat{b}(\omega, 0) d\omega. \quad (2.6)$$

Using this, and the commutation relation $[\hat{b}(\omega), \hat{b}^\dagger(\tilde{\omega})] = \delta(\omega - \tilde{\omega})$, we obtain,

$$[\hat{b}_{in}(t), \hat{b}_{in}^\dagger(s)] = \frac{1}{2\pi} \int_{\Omega \times \Omega} d\omega d\tilde{\omega} e^{-i(\omega t - \tilde{\omega} s)} [\hat{b}_{in}(\omega), \hat{b}_{in}^\dagger(\tilde{\omega})], \quad (2.7a)$$

$$= \frac{1}{2\pi} \int_{\Omega} d\omega e^{-i\omega(t-s)}, \quad (2.7b)$$

$$\approx e^{-i\omega_0(t-s)} \delta(t-s), \quad (2.7c)$$

where to get the Dirac delta function we make use of the large bandwidth or short correlation time of the bath, $\Delta_B^{-1} = \tau_c \approx 0$.

From the definition of the input field, we can simplify the first integral of Eq. (2.5),

$$\begin{aligned} \int_{\Omega} \left\{ e^{i\omega t} \hat{b}^\dagger(\omega, 0) [\hat{c}_S, \hat{O}_S] - [\hat{c}_S^\dagger, \hat{O}_S] e^{-i\omega t} \hat{b}(\omega, 0) \right\} d\omega &= \sqrt{2\pi} \hat{b}_{in}^\dagger(t) [\hat{c}_S, \hat{O}_S] \\ &\quad - \sqrt{2\pi} [\hat{c}_S^\dagger, \hat{O}_S] \hat{b}_{in}(t). \end{aligned} \quad (2.8)$$

In the second integral of Eq. (2.5) the operator $\hat{c}_S(s)$ just contributes for short times $|t-s| \leq \tau_c$. Using this, we approximate its time evolution by,

$$\hat{c}_S(s) \approx e^{-i\omega_0(t-s)} \hat{c}_S(t). \quad (2.9)$$

So,

$$\int_{\Omega} d\omega \int^t ds e^{-i\omega(t-s)} \hat{c}_S(s) \approx \hat{c}_S(t) \int_{\Omega} d\omega \int^t ds e^{-i(\omega-\omega_0)(t-s)}, \quad (2.10a)$$

$$\approx 2\pi \hat{c}_S(t) \int^t \delta(t-s) ds, \quad (2.10b)$$

$$= \pi \hat{c}_S(t), \quad (2.10c)$$

$$\int_{\Omega} d\omega \int^t ds e^{i\omega(t-s)} \hat{c}_S^\dagger(s) \approx \pi \hat{c}_S^\dagger(t). \quad (2.10d)$$

Using those expressions we can write,

$$\begin{aligned} \int_{\Omega} d\omega \int^t ds \left\{ e^{i\omega(t-s)} \hat{c}_S^\dagger(s) [\hat{c}_S, \hat{O}_S] - [\hat{c}_S^\dagger, \hat{O}_S] e^{-i\omega(t-s)} \hat{c}_S(s) \right\} &= \pi \hat{c}_S^\dagger(t) [\hat{c}_S, \hat{O}_S] \\ &\quad - \pi [\hat{c}_S^\dagger, \hat{O}_S] \hat{c}_S(t). \end{aligned} \quad (2.11)$$

Now, we define the damping coefficient as,

$$\Gamma_S := 2\pi \lambda^2, \quad (2.12)$$

which is also called the decay rate. Then, Eq. (2.5) under the Markov approximation is,

$$\frac{d\hat{O}_S}{dt} = i [\hat{H}_S, \hat{O}_S] - [\hat{O}_S, \hat{c}_S^\dagger] \left(\frac{\Gamma_S}{2} \hat{c}_S + \sqrt{\Gamma_S} \hat{b}_{in} \right) - \left(\frac{\Gamma_S}{2} \hat{c}_S^\dagger + \sqrt{\Gamma_S} \hat{b}_{in}^\dagger \right) [\hat{c}_S, \hat{O}_S], \quad (2.13)$$

which is the general form of the QLE for an arbitrary system operator \hat{O}_S .

2.1.2 Linearized optomechanical system

We derive the QLEs for an optomechanical system under a linearized approach given in Sec. 1.2.1. For the notation of Eq. (2.13), we split the operators of the system into its semiclassical field amplitude plus a quantum fluctuation,

$$\hat{O}_S \rightarrow \langle \hat{O}_S \rangle + \delta \hat{O}_S, \quad (2.14a)$$

$$\hat{c}_S \rightarrow \langle \hat{c}_S \rangle + \delta \hat{c}_S. \quad (2.14b)$$

We assumed that both contributions are time-dependent. With this expressions, we also affect the Hamiltonian of the system. As a result, we obtain contributions that are linear combination of individual operators, pair of multiplied operators and so on. Also, we separate the obtained differential equation in two: one for the semiclassical field amplitude which contains scalar functions and the other for the quantum fluctuations which contains operators,

$$\frac{d}{dt} \langle \hat{O}_S \rangle = i \left[\hat{H}_S^{(1)}, \delta \hat{O}_S \right] - \frac{\gamma}{2} \langle \hat{c}_S \rangle \left[\delta \hat{O}_S, \delta \hat{c}_S^\dagger \right] - \frac{\gamma}{2} \langle \hat{c}_S^\dagger \rangle \left[\delta \hat{O}_S, \delta \hat{c}_S \right], \quad (2.15a)$$

$$\begin{aligned} \frac{d}{dt} \delta \hat{O}_S = & i \left[\hat{H}_S^{(2)} + \dots, \delta \hat{O}_S \right] - \left[\delta \hat{O}_S, \delta \hat{c}_S^\dagger \right] \left(\frac{\gamma}{2} \delta \hat{c}_S + \sqrt{\gamma} \hat{b}_{in} \right) \\ & - \left(\frac{\gamma}{2} \delta \hat{c}_S^\dagger + \sqrt{\gamma} \hat{b}_{in}^\dagger \right) \left[\delta \hat{O}_S, \delta \hat{c}_S \right]. \end{aligned} \quad (2.15b)$$

We define Hamiltonians for the contributions mentioned before: for the one proportional to individual operators is $\hat{H}_S^{(1)}$, while $\hat{H}_S^{(2)}$ is proportional to pairs of multiplied operators, and so on. There is also a contribution which is conformed by scalar functions, $\hat{H}_S^{(0)}$, and because of that, it does not play any roll in the differential equations.

For the optomechanical system described by the Hamiltonian (1.4), the operators \hat{O}_S and \hat{c}_S can be any of \hat{a} , \hat{a}^\dagger , \hat{b} , \hat{b}^\dagger . For the purpose of the next chapter, we use a slightly changed version of Eqs. (1.2),

$$\hat{a} \rightarrow \alpha e^{i\phi} + \hat{c}, \quad (2.16a)$$

$$\hat{b} \rightarrow \beta + \hat{d}. \quad (2.16b)$$

The justification for this change comes from Eq. (1.6a). There, we see the explicit dependence of the EM semiclassical field amplitude on the driving-laser phase. Also, we assume that the semiclassical field amplitudes, quantum fluctuations and driving-laser phase are time-dependent, *i. e.*, $\phi = \phi(t)$. Then, the Hamiltonian (1.4) becomes the sum of:

$$\hat{H}_S^{(0)} = -\Delta |\alpha|^2 + \omega_m |\beta|^2 + i \frac{\varepsilon}{2} (\alpha^* - \alpha), \quad (2.17a)$$

$$\hat{H}_S^{(1)} = (i\varepsilon/2 - \Delta) e^{i\phi} \hat{c}^\dagger + (\omega_m \beta + g_0 |\alpha|^2) \hat{d}^\dagger + H.C., \quad (2.17b)$$

$$\hat{H}_S^{(2)} = -\Delta \hat{c}^\dagger \hat{c} + \omega_m \hat{d}^\dagger \hat{d} + g (e^{i\varphi} \hat{c}^\dagger + e^{-i\varphi} \hat{c}) (\hat{d}^\dagger + \hat{d}), \quad (2.17c)$$

$$\hat{H}_S^{(3)} = g_0 \hat{c}^\dagger \hat{c} (\hat{d}^\dagger + \hat{d}), \quad (2.17d)$$

where we define the auxiliary phase function $\varphi = \varphi(t) = \phi + \arg(\alpha)$ which inherits the time-dependence from the driving laser phase, ϕ . Also, we use the definition for the detuning

in Sec. 1.2.1, $\Delta = \omega_p - \omega_c - 2g_0 \text{Re}(\beta)$. We see that $\hat{H}_S^{(2)}$ is the linearized optomechanical Hamiltonian \hat{H}_{lin} , Eq. (1.5). Under the assumption of strong laser driving, we omit the contribution due to $\hat{H}_S^{(3)}$.

The equations obtained, following the Eqs. (2.15), for the linearized optomechanical system are,

$$\frac{d}{dt} \tilde{\alpha} = - \left(\frac{\kappa}{2} - i \Delta \right) \tilde{\alpha} + \frac{\varepsilon}{2}, \quad (2.18a)$$

$$\frac{d}{dt} \beta = - \left(\frac{\gamma}{2} + i \omega_m \right) \beta - i g_0 |\alpha|^2, \quad (2.18b)$$

$$\frac{d}{dt} \hat{c} = - \left(\frac{\kappa}{2} - i \Delta \right) \hat{c} - i e^{i\varphi} g \left(\hat{d}^\dagger + \hat{d} \right) - \sqrt{\kappa} \hat{c}_{in}, \quad (2.18c)$$

$$\frac{d}{dt} \hat{d} = - \left(\frac{\gamma}{2} + i \omega_m \right) \hat{d} - i g \left(e^{i\varphi} \hat{c}^\dagger + e^{-i\varphi} \hat{c} \right) - \sqrt{\gamma} \hat{d}_{in}, \quad (2.18d)$$

where $\tilde{\alpha} = e^{i\phi} \alpha$ and the cavity (mechanical) decay rate is κ (γ). The hermitian conjugated of this equations give us the differential equations for α^* , β^* , \hat{c}^\dagger and \hat{d}^\dagger .

Like in Sec. 1.2.1, we apply the RWA for the detuning sidebands, $\Delta = \pm \omega_m$. We arrange the resulting coupled QLEs for the quantum fluctuations in matrix form,

Red-detuning ($\Delta = -\omega_m$),

$$\frac{d}{dt} \begin{pmatrix} \hat{c} \\ \hat{d} \end{pmatrix} = - \begin{pmatrix} \kappa/2 + i \omega_m & i g e^{i\varphi} \\ i g e^{-i\varphi} & \gamma/2 + i \omega_m \end{pmatrix} \begin{pmatrix} \hat{c} \\ \hat{d} \end{pmatrix} - \begin{pmatrix} \sqrt{\kappa} \hat{c}_{in} \\ \sqrt{\gamma} \hat{d}_{in} \end{pmatrix}, \quad (2.19)$$

Blue-detuning ($\Delta = +\omega_m$),

$$\frac{d}{dt} \begin{pmatrix} \hat{c} \\ \hat{d}^\dagger \end{pmatrix} = - \begin{pmatrix} \kappa/2 - i \omega_m & i g e^{i\varphi} \\ -i g e^{-i\varphi} & \gamma/2 - i \omega_m \end{pmatrix} \begin{pmatrix} \hat{c} \\ \hat{d}^\dagger \end{pmatrix} - \begin{pmatrix} \sqrt{\kappa} \hat{c}_{in} \\ \sqrt{\gamma} \hat{d}_{in}^\dagger \end{pmatrix}. \quad (2.20)$$

The RWA in this sidebands helps us to reduce from four to just two QLEs coupled. Then, it is easier to calculate analytically the time-evolution of the quantum fluctuations.

The time-evolution of the semiclassical field amplitudes is given by Eqs. (2.18a) and (2.18b). These equations will be used in the Sec. 3.3 for the time evolution under a smooth driving-laser phase. Additionally, we obtain the semiclassical steady-state values for the EM and mechanical fields, *i. e.*, values when $\partial_t (\alpha_{ss}, \beta_{ss}) = (0, 0)$,

$$\alpha_{ss} = \frac{e^{-i\phi_{ss}} \varepsilon}{\kappa - i 2 \Delta}, \quad (2.21a)$$

$$\beta_{ss} = \frac{i g_0 |\alpha|^2}{\gamma/2 + i \omega_m}, \quad (2.21b)$$

where ϕ_{ss} is the steady value of the driving-laser phase. This expressions are similar to those found in Sec. 1.2.1, but here the decay rates of both fields were taken into account.

The bistability phenomena is observed just for negative values of the laser detuning [24], $\omega_p - \omega_c =: \Delta_0 < 0$. Additionally, we approximate the detuning as $\Delta \approx \Delta_0$ under the

assumptions: positive laser detuning, $\Delta_0 > 0$ and small values of the mechanical decay rate, $\gamma/\omega_m \ll 1$, and the enhanced optomechanical coupling, $g/\omega_m \ll 1$. Then, the approximated semiclassical steady-state for the EM field amplitude is,

$$\alpha_{ss} \approx \frac{e^{-i\phi_{ss}} \varepsilon}{\kappa + i2(\omega_c - \omega_p)}, \quad (2.22)$$

which corresponds to a cavity driven by a laser.

2.2 Master Equation

Another approach to describe the time evolution of the quantum system coupled to a bath is through the density operator, $\hat{\rho}$. We derive the master equation for the degrees of freedom of our system of interest, *i. e.*, the equation for $\hat{\rho}_S = \text{Tr}_B \{\hat{\rho}\}$. We start with the von Neumann equation,

$$\frac{d\hat{\rho}(t)}{dt} = -i \left[\hat{H}_S + \hat{H}_B + \hat{H}_I, \hat{\rho}(t) \right], \quad (2.23)$$

where the notation for the Hamiltonians is the same as in the previous section. Here, we consider a more general form of the interaction Hamiltonian,

$$\hat{H}_I = \sum_{\eta} \hat{S}_{\eta} \otimes \hat{B}_{\eta}, \quad (2.24)$$

where the operators \hat{S}_{η} (\hat{B}_{η}) stands for the system (bath).

We move to the interaction picture with respect to $\hat{H}_0 = \hat{H}_S + \hat{H}_B$, *i. e.*, $\tilde{\rho}(t) = e^{i\hat{H}_0 t} \hat{\rho} e^{-i\hat{H}_0 t}$. Then, we get,

$$\frac{d\tilde{\rho}(t)}{dt} = -i \left[e^{i\hat{H}_0 t} \hat{H}_I e^{-i\hat{H}_0 t}, \tilde{\rho}(t) \right], \quad (2.25a)$$

$$= -i \left[\hat{H}'_I(t), \tilde{\rho}(t) \right]. \quad (2.25b)$$

This equation can be formally integrated to obtain,

$$\tilde{\rho}(t) = \tilde{\rho}(0) - i \int_0^t \left[\hat{H}'_I(t'), \tilde{\rho}(t') \right] dt', \quad (2.26a)$$

$$= \tilde{\rho}(0) - i \int_0^t \left[\hat{H}'_I(t'), \tilde{\rho}(0) \right] dt' - \int_0^t dt' \int_0^{t'} dt'' \left[\hat{H}'_I(t'), \left[\hat{H}'_I(t''), \tilde{\rho}(t'') \right] \right]. \quad (2.26b)$$

In order to obtain the equation for our system of interest we trace over the bath degrees of freedom,

$$\begin{aligned} \tilde{\rho}_S(t) &= \tilde{\rho}_S(0) - i \int_0^t dt' \text{Tr}_B \left\{ \left[\hat{H}'_I(t'), \tilde{\rho}(0) \right] \right\} \\ &\quad - \int_0^t dt' \int_0^{t'} dt'' \text{Tr}_B \left\{ \left[\hat{H}'_I(t'), \left[\hat{H}'_I(t''), \tilde{\rho}(t'') \right] \right] \right\}, \end{aligned} \quad (2.27)$$

which is, to this point, an exact result.

2.2.1 Born and Markov approximations

To simplify Eq. (2.27), we assume a sufficiently weak interaction between the system of interest and the bath, and because of the large number of degrees of freedom of the environment, it is weakly perturbed by the system. Therefore, we can write approximatively,

$$\tilde{\rho}(t) \approx \tilde{\rho}_S(t) \otimes \tilde{\rho}_B(0), \quad (2.28)$$

where $\tilde{\rho}_B(0)$ represents the stationary state of the bath. The latter is the so-called Born approximation and using it we can evaluate the trace in the first integral of Eq. (2.27),

$$\text{Tr}_B \left\{ \left[\hat{H}'_I(t'), \tilde{\rho}(0) \right] \right\} = \text{Tr}_B \left\{ \left[\hat{H}'_I(t'), \tilde{\rho}_S(0) \otimes \tilde{\rho}_B(0) \right] \right\}, \quad (2.29a)$$

$$= \text{Tr}_B \left\{ \left[\sum_{\eta} \tilde{S}_{\eta}(t') \otimes \tilde{B}_{\eta}(t'), \tilde{\rho}_S(0) \otimes \tilde{\rho}_B(0) \right] \right\}, \quad (2.29b)$$

$$= \sum_{\eta} \text{Tr}_B \left\{ \tilde{B}_{\eta}(t') \tilde{\rho}_B(0) \right\} \left[\tilde{S}_{\eta}(t'), \tilde{\rho}_S(0) \right], \quad (2.29c)$$

$$= \sum_{\eta} \langle \tilde{B}_{\eta}(t') \rangle \left[\tilde{S}_{\eta}(t'), \tilde{\rho}_S(0) \right]. \quad (2.29d)$$

Here, we require the value $\langle \tilde{B}_{\eta}(t') \rangle$ which for many situations it is equal to zero, in consequence the first integral in Eq. (2.27) is zero under the Born approximation. If we found $\langle \tilde{B}_{\eta}(t') \rangle \neq 0$, we can absorb the finite value by making the replacements,

$$\hat{H}_S \rightarrow \hat{H}_S + \sum_{\eta} \hat{S}_{\eta} \langle \hat{B}_{\eta} \rangle, \quad (2.30a)$$

$$\hat{H}_I \rightarrow \sum_{\eta} \hat{S}_{\eta} \left(\hat{B}_{\eta} - \langle \hat{B}_{\eta} \rangle \right), \quad (2.30b)$$

in Eq. (2.23), *i. e.*, we just add and subtract the same quantity to the original Hamiltonian. Then, we should get in Eq. (2.29d): $\langle \tilde{B}_{\eta}(t') \rangle \rightarrow \langle \tilde{B}_{\eta}(t') - \langle \tilde{B}_{\eta}(t') \rangle \rangle = 0$. So, without loss of generality we can assume $\langle \tilde{B}_{\eta}(t') \rangle = 0$.

Taking the time derivative of Eq. (2.27) under the Born approximation, we end up with,

$$\frac{d\tilde{\rho}_S(t)}{dt} = - \int_0^t dt' \text{Tr}_B \left\{ \left[\hat{H}'_I(t), \left[\hat{H}'_I(t'), \tilde{\rho}_S(t') \otimes \tilde{\rho}_B(0) \right] \right] \right\}, \quad (2.31)$$

which is known as the Nakajima-Zwanzig equation. We observe that it is non-local in time, *i. e.*, the derivative of $\tilde{\rho}_S(t)$ at time t depends on earlier times, $\tilde{\rho}_S(t')$ with $0 < t' < t$.

We invoke the short correlation time, $\Delta_B^{-1} = \tau_c \approx 0$, to approximatively set $\tilde{\rho}_S(t') \approx \tilde{\rho}_S(t)$. Then,

$$- \frac{d\tilde{\rho}_S(t)}{dt} \approx \int_{-\infty}^t dt' \text{Tr}_B \left\{ \left[\hat{H}'_I(t), \left[\hat{H}'_I(t'), \tilde{\rho}_S(t) \otimes \tilde{\rho}_B(0) \right] \right] \right\}, \quad (2.32a)$$

$$= \int_0^{\infty} d\tau \text{Tr}_B \left\{ \left[\hat{H}'_I(t), \left[\hat{H}'_I(t - \tau), \tilde{\rho}_S(t) \otimes \tilde{\rho}_B(0) \right] \right] \right\}, \quad (2.32b)$$

where we made the change $t' = t - \tau$. Expanding the commutator and using Eq. (2.24), we can write,

$$\begin{aligned}
 -\frac{d\tilde{\rho}_S(t)}{dt} &\approx \int_0^\infty d\tau \langle \tilde{B}_\mu(t) \tilde{B}_\eta(t-\tau) \rangle \left\{ \tilde{S}_\mu(t) \tilde{S}_\eta(t-\tau) \tilde{\rho}_S(t) - \tilde{S}_\eta(t-\tau) \tilde{\rho}_S(t) \tilde{S}_\mu(t) \right\} \\
 &\quad + \int_0^\infty d\tau \langle \tilde{B}_\eta(t-\tau) \tilde{B}_\mu(t) \rangle \left\{ \tilde{\rho}_S(t) \tilde{S}_\eta(t-\tau) \tilde{S}_\mu(t) - \tilde{S}_\mu(t) \tilde{\rho}_S(t) \tilde{S}_\eta(t-\tau) \right\},
 \end{aligned} \tag{2.33}$$

where we omitted the sum sign $\sum_{\mu,\eta}$. In the case when the bath is a vacuum or thermal state, the correlations $\langle \tilde{B}_\mu(t-\tau) \tilde{B}_\mu(t) \rangle = 0$, *i. e.*, we just consider those terms of the sum where $\mu \neq \eta$.

We proceed considering an interaction Hamiltonian of the form, with $\hbar = 1$,

$$\hat{H}'_I(t) = \sqrt{\gamma} \left[e^{-i\omega_0 t} \hat{c} \hat{B}^\dagger(t) + e^{i\omega_0 t} \hat{c}^\dagger \hat{B}(t) \right], \tag{2.34}$$

from which we set the operators $\tilde{S}_1(t) = e^{-i\omega_0 t} \hat{c}$, $\tilde{B}_1(t) = \sqrt{\gamma} \hat{B}^\dagger(t)$, $\tilde{S}_2(t) = e^{i\omega_0 t} \hat{c}^\dagger$ and $\tilde{B}_2(t) = \sqrt{\gamma} \hat{B}(t)$. The equation for $\tilde{\rho}_S(t)$ contains eight integrals which are related with the expressions,

$$\langle \hat{B}^\dagger(t) \hat{B}(t-\tau) \rangle = \langle \hat{B}^\dagger(\tau) \hat{B}(0) \rangle = \langle \hat{B}^\dagger(0) \hat{B}(\tau) \rangle^* = \langle \hat{B}^\dagger(t-\tau) \hat{B}(t) \rangle, \tag{2.35a}$$

$$\langle \hat{B}(t) \hat{B}^\dagger(t-\tau) \rangle = \langle \hat{B}(\tau) \hat{B}^\dagger(0) \rangle = \langle \hat{B}(0) \hat{B}^\dagger(\tau) \rangle^* = \langle \hat{B}(t-\tau) \hat{B}^\dagger(t) \rangle, \tag{2.35b}$$

where we used the properties of the thermal density matrix for the bath, $\hat{\rho}_B(0) = \hat{\rho}_{th}(N_{th})$, with N_{th} the equilibrium thermal occupancy number. We define the functions,

$$I_+(\omega) = 2\gamma \int_0^\infty d\tau e^{-i\omega\tau} \langle \hat{B}^\dagger(\tau) \hat{B}(0) \rangle, \tag{2.36a}$$

$$I_-(\omega) = 2\gamma \int_0^\infty d\tau e^{i\omega\tau} \langle \hat{B}(\tau) \hat{B}^\dagger(0) \rangle. \tag{2.36b}$$

Then, we can write Eq. (2.33) like,

$$\begin{aligned}
 -\frac{d\tilde{\rho}_S}{dt} &= \frac{i}{2} \left[\text{Im} \{I_+(\omega_0)\} \hat{c} \hat{c}^\dagger + \text{Im} \{I_-(\omega_0)\} \hat{c}^\dagger \hat{c}, \tilde{\rho}_S \right] \\
 &\quad - \frac{\text{Re} \{I_+(\omega_0)\}}{2} (2\hat{c}^\dagger \tilde{\rho}_S \hat{c} - \hat{c} \hat{c}^\dagger \tilde{\rho}_S - \tilde{\rho}_S \hat{c} \hat{c}^\dagger) - \frac{\text{Re} \{I_-(\omega_0)\}}{2} (2\hat{c} \tilde{\rho}_S \hat{c}^\dagger - \hat{c}^\dagger \hat{c} \tilde{\rho}_S - \tilde{\rho}_S \hat{c}^\dagger \hat{c}).
 \end{aligned} \tag{2.37a}$$

In the Schrödinger picture, this equation is,

$$\begin{aligned}
 \frac{d\hat{\rho}_S}{dt} &= -i \left[\hat{H}_S + \hat{H}_{xtr}, \hat{\rho}_S \right] + \frac{\text{Re} \{I_+(\omega_0)\}}{2} (2\hat{c}^\dagger \hat{\rho}_S \hat{c} - \hat{c} \hat{c}^\dagger \hat{\rho}_S - \hat{\rho}_S \hat{c} \hat{c}^\dagger) \\
 &\quad + \frac{\text{Re} \{I_-(\omega_0)\}}{2} (2\hat{c} \hat{\rho}_S \hat{c}^\dagger - \hat{c}^\dagger \hat{c} \hat{\rho}_S - \hat{\rho}_S \hat{c}^\dagger \hat{c}),
 \end{aligned} \tag{2.38}$$

with $\hat{H}_{xtr} = \text{Im} \{I_+(\omega_0)\} \hat{c} \hat{c}^\dagger + \text{Im} \{I_-(\omega_0)\} \hat{c}^\dagger \hat{c}$.

Now, due to the thermal state of the bath, we have,

$$\langle \hat{B}^\dagger(\tau) \hat{B}(0) \rangle \approx N_{th} e^{i\omega_0 \tau} \delta(\tau), \quad (2.39a)$$

$$\langle \hat{B}(\tau) \hat{B}^\dagger(0) \rangle \approx (N_{th} + 1) e^{-i\omega_0 \tau} \delta(\tau). \quad (2.39b)$$

This implies that $I_+(\omega_0) = \gamma N_{th}$ and $I_-(\omega_0) = \gamma(N_{th} + 1)$, *i. e.*, $\text{Im} \{I_\pm(\omega_0)\} = 0$. Finally, we obtain the master equation:

$$\begin{aligned} \frac{d\hat{\rho}_S}{dt} = & -i [\hat{H}_S, \hat{\rho}_S] + \frac{\gamma N_{th}}{2} (2\hat{c}^\dagger \tilde{\rho}_S \hat{c} - \hat{c} \hat{c}^\dagger \tilde{\rho}_S - \tilde{\rho}_S \hat{c} \hat{c}^\dagger) \\ & + \frac{\gamma (N_{th} + 1)}{2} (2\hat{c} \tilde{\rho}_S \hat{c}^\dagger - \hat{c}^\dagger \hat{c} \tilde{\rho}_S - \tilde{\rho}_S \hat{c}^\dagger \hat{c}), \end{aligned} \quad (2.40)$$

which is also named as the master equation in Lindblad form or Lindblad master equation. This can be written like $\partial_t \hat{\rho}_S = \mathcal{L} \hat{\rho}_S$, where \mathcal{L} is a superoperator called Liouvillian, and its formal solution is $\hat{\rho}_S(t) = e^{\mathcal{L}t} \hat{\rho}_S(0)$. In the case when the number of the operators for the system is larger than one, the Lindblad master equation takes the form,

$$\frac{d\hat{\rho}_S}{dt} = -i [\hat{H}_S, \hat{\rho}_S] + \sum_k \left\{ \frac{\gamma_k N_k}{2} \hat{L}[c_k^\dagger] \hat{\rho}_S + \frac{\gamma_k (N_k + 1)}{2} \hat{L}[c_k] \hat{\rho}_S \right\}, \quad (2.41)$$

where we define the superoperator $\hat{L}[O_k] \hat{\rho}_S = 2\hat{O}_k \hat{\rho}_S \hat{O}_k^\dagger - (\hat{O}_k^\dagger \hat{O}_k \hat{\rho}_S + \hat{\rho}_S \hat{O}_k^\dagger \hat{O}_k)$. Also, for every operator O_k corresponds a decay rate γ_k and a equilibrium thermal occupancy number N_k .

2.3 Composite pulse sequence for a qubit

To achieve population inversion in a qubit, we apply a π -pulse with a coherent field on resonance with constant phase. The technique fails if the pulse area, the frequencies or the phase conditions do not hold for the whole process, *i. e.*, this technique is very sensitive to systematic errors on those parameters. One option to have a more accurate control of the inversion is the use of a sequence of π -pulses with appropriately chosen phases [100, 107]. In the Bloch sphere representation [108], the action of those phases can be seen as composed rotations which reduce the sensitivity to the systematic errors.

Here we review the formalism given in Ref. [100–103] for the so-called broadband (BB) composite sequence, *i. e.*, when the population inversion occurs with a π -pulse. The longer the BB sequence, the flatter the inversion profile around the area π . The time-evolution of the qubit can be visualized using the Bloch sphere representation, where the qubit's quantum-state is mapped to a point on the surface of the sphere and its evolution produces a path.

We consider a qubit with transition frequency ω_a driven by a laser with frequency ω_l . The Hamiltonian in the interaction picture is, with $\hbar = 1$,

$$\hat{H}(t) = \frac{\Omega(t) e^{-iD(t)}}{2} \hat{\sigma}_+ + \frac{\Omega^*(t) e^{iD(t)}}{2} \hat{\sigma}_-, \quad (2.42)$$

with $D(t) = \int_{t_i}^t \Delta(t') dt'$, where $\Delta = \omega_a - \omega_l$ is the detuning between the laser and qubit frequencies. We used the standard definition for the Pauli matrices. The Rabi frequency $\Omega(t)$ parametrizes the coupling between the laser field and the qubit. The time evolution of the qubit's quantum state, $|c(t)\rangle$, follows the Schrödinger equation,

$$i \frac{d}{dt} |c(t)\rangle = \hat{H}(t) |c(t)\rangle. \quad (2.43)$$

From this equation, we obtain the evolution operator \hat{U} , *i. e.*, $|c(t)\rangle = \hat{U}(t) |c(t_i)\rangle$ and its matrix form is,

$$\hat{U} = \begin{pmatrix} a & b \\ -b^* & a^* \end{pmatrix}, \quad (2.44)$$

with $|a|^2 + |b|^2 = 1$. In the case of exact resonance, $\Delta = 0$, there is an analytic expression for the matrix elements,

$$a = \cos(A/2), \quad (2.45a)$$

$$b = -i \sin(A/2), \quad (2.45b)$$

where we defined the pulse area $A = \int_{t_i}^t \Omega(t') dt'$ and we assumed $\Omega(t)$ is a real function. The transition probability is given by $p = |b|^2 = \sin^2(A/2)$. Complete population inversion occurs for $A = \pi$, for the so-called π -pulse, alternatively for odd-integer multiples of π . The inversion is sensitive for small deviation, $\epsilon < 1$, in the value π , *i. e.*, $A = \pi(1 + \epsilon)$. It causes an error in the inversion of order $\mathcal{O}(\epsilon^2)$, then $p = 1 - (\pi\epsilon/2)^2 + \mathcal{O}(\epsilon^4)$.

The sensitivity to errors can be reduced by replacing the single π -pulse by a composite pulse sequence. A constant phase shift to the Rabi frequency, $\Omega(t) \rightarrow \Omega(t) e^{i\phi}$, causes a phase shift in the evolution operator,

$$\hat{U}_\phi(A) = \begin{pmatrix} a & b e^{-i\phi} \\ -b^* e^{i\phi} & a^* \end{pmatrix}. \quad (2.46)$$

The phase shift added can be seen as a rotation in the Bloch sphere around the z -axis. We must not confuse the phase shift ϕ with the driving-laser phase of the optomechanical system.

The evolution operator for a sequence of N pulses, each one with area A_k and phase ϕ_k , can be written by the product of the correspondent for every pulse,

$$\hat{U}^{(N)} = \hat{U}_{\phi_N}(A_N) \hat{U}_{\phi_{N-1}}(A_{N-1}) \cdots \hat{U}_{\phi_2}(A_2) \hat{U}_{\phi_1}(A_1). \quad (2.47)$$

We consider an odd number of pulses for the BB composite sequence because it is necessary and odd multiple of π to produce complete population inversion. For the composite pulse sequence, we assume every pulse area is the same, A , and the phases are our free parameters. Also, we require a reversal symmetry property for the phases, *i. e.*, they obey $\phi_k = \phi_{N+1-k}$. Because it is only relevant the relative phase of the pulses, we can set $\phi_1 = \phi_N = 0$, which implies that we have just $(N-1)/2$ free values of the phases. The set $\{\pm\phi_k \mid k = 2, \dots, (N+1)/2\}$ is the solution for the control problem

N	Phases (units of π/N)																
3																	
						0	2	0									
5						0	4	2	4	0							
7					0	6	4	8	4	6	0						
9				0	8	6	12	8	12	6	8	0					
11			0	10	8	16	12	18	12	16	8	10	0				
13		0	12	10	20	16	24	18	24	16	20	10	12	0			
15		0	14	12	24	20	30	24	32	24	30	20	24	12	14	0	
17	0	16	14	28	24	36	30	40	32	40	30	36	24	28	14	16	0

Table 2.1: Value of the phases for the first eight BB composite sequences at resonance.

In order to obtain the set $\{\pm\phi_k\}$ which creates the desire flat profile for the population inversion around the area π , it is necessary to nullify the matrix element $U_{11}^{(N)}$, alternatively, maximize $U_{12}^{(N)}$. Then, we must have the conditions:

$$U_{11}^{(N)}(A = \pi) = 0, \quad (2.48a)$$

$$\left. \frac{\partial^S U_{11}^{(N)}}{\partial A} \right|_{A=\pi} = 0, \quad (2.48b)$$

for $S = 1, \dots, (N-1)/2$. As alternative, we have $\partial_A^S U_{12}^{(N)}|_{A=\pi} = 0$ and $U_{12}^{(N)}(A = \pi) = 1$. Solving the set of those equations, we found the values for the phases with analytic form,

$$\phi_k = \left[N + 1 - 2 \text{Floor} \left(\frac{k+1}{2} \right) \right] \text{Floor} \left(\frac{k}{2} \right) \frac{\pi}{N}, \quad (2.49)$$

where $\text{Floor}(x)$ is the function which returns the integer part of x . In Table 2.1 we show the value of the phases for the first eight sequences. With that phase sequence, an error ϵ in every pulse area produces a transition probability $p = 1 - (\pi\epsilon/2)^{2N} + \mathcal{O}(\epsilon^{2N+2})$, then $p \rightarrow 1$ for $N \rightarrow \infty$.

In the process to develop the BB composite sequence we assumed a time dependency of the Rabi frequency and a constant laser detuning. This sequence is also suitable when we have the conditions [101]:

$$\Omega(t) = \Omega(-t), \quad (2.50a)$$

$$\Delta(t) = -\Delta(-t). \quad (2.50b)$$

Even though we considered just in deviations of the pulse area, a BB composite sequence can be derived in order to reduce sensitivity of the inversion due to errors of the detuning. We don't reproduce that process here because it is not our target to use it.

2.4 \mathcal{PT} -symmetry

One postulate of quantum mechanics stipulates that for every measurable quantity corresponds a linear Hermitian operator [109]. The eigenvalues of those operators are real numbers, the measurable quantities. The Hamiltonian, \hat{H} , in the Schrödinger equation gives the

total energy for time-dependent systems and its time-evolution. This implies that \hat{H} must be Hermitian, $\hat{H} = \hat{H}^\dagger$. But some years ago, it was found that certain class of non-Hermitian operators have real eigenvalues [110, 111]. These operators are invariant under space-time reflection, \mathcal{PT} -symmetry. The operator \mathcal{P} stands for the space reflection and \mathcal{T} for the time-reflection. If \hat{x} and \hat{p} represents the coordinate and momentum operators respectively, the effects of \mathcal{P} and \mathcal{T} are,

$$\mathcal{P} \hat{x} \mathcal{P} = -\hat{x}, \quad \mathcal{P} \hat{p} \mathcal{P} = -\hat{p}, \quad (2.51a)$$

$$\mathcal{T} \hat{x} \mathcal{T} = \hat{x}, \quad \mathcal{T} \hat{p} \mathcal{T} = -\hat{p}. \quad (2.51b)$$

The time-reflection changes the sign in the complex number, $i \rightarrow -i$. From those expressions, we know that \mathcal{P} is a linear operator and \mathcal{T} is antilinear. Also, the relations $\mathcal{P}^2 = \mathcal{T}^2 = 1$ are obtained and more interesting,

$$[\hat{H}, \mathcal{PT}] = 0. \quad (2.52)$$

It can also be written like $\hat{H} = \mathcal{PT} \hat{H} \mathcal{PT} = \hat{H}_{\mathcal{PT}}$. These expressions are the core of research in \mathcal{PT} -symmetric Hamiltonians. Then, the mathematical condition $\hat{H} = \hat{H}^\dagger$ can be replaced by $\hat{H} = \hat{H}_{\mathcal{PT}}$. With this, non-Hermitian descriptions of quantum systems can be accepted if its respective Hamiltonian possesses \mathcal{PT} -symmetry.

As an example, the family of \mathcal{PT} -symmetric Hamiltonians $\hat{H} = \hat{p}^2 + \hat{x}^2 (i\hat{x})^\epsilon$, with $\epsilon \in \mathbb{R}$. This Hamiltonian possesses eigenvalues that are real and positive for $\epsilon \geq 0$, but when $\epsilon < 0$ the eigenvalues are complex [111]. This characteristic defines the so-called unbroken and broken regions of the \mathcal{PT} -symmetry, *i. e.*, the real eigenvalues are found in the unbroken region while the complex eigenvalues correspond to the broken region.

2.4.1 Gain-loss system

The classical simulation of non-Hermitian quantum mechanics is possible in photonics. This is based on the equivalence between the Schrödinger and Helmholtz equations [112, 113]. The \mathcal{PT} -symmetric quantum potential $\hat{V}(\hat{x}) = \hat{V}^\dagger(-\hat{x})$ corresponds to a complex refractive index $n(x) = n^*(-x)$. The latter implies that amount of losses must be equal to the gain. Particularly, a two-waveguide coupler is described by two coupled differential equations which can be written like [114],

$$-i \frac{d}{d\zeta} \begin{pmatrix} \mathcal{E}_1 \\ \mathcal{E}_2 \end{pmatrix} = \begin{pmatrix} i\tilde{\Gamma} & 1 \\ 1 & -i\tilde{\Gamma} \end{pmatrix} \begin{pmatrix} \mathcal{E}_1 \\ \mathcal{E}_2 \end{pmatrix}, \quad (2.53)$$

where is defined an scaled propagation distance $\zeta = \tilde{g}z$ with $\tilde{g} \in \mathbb{R}$ as the waveguide coupling constant and $z \geq 0$ the propagation distance. The effective complex amplitude at each waveguide is \mathcal{E}_j and an effective refractive index $\tilde{\Gamma} \in \mathbb{R}$. With this model, the propagation of the amplitudes exhibits different behaviours depending on whether the two eigenvalues,

$$m_\pm = \pm \sqrt{1 - \tilde{\Gamma}^2}, \quad (2.54)$$

are real or imaginary. This leads to the following regimes [115]:

Unbroken \mathcal{PT} -symmetry when $|\tilde{\Gamma}| < 1$. An oscillatory behaviour is expected. The eigenvalues, m_{\pm} , are real numbers and its correspondent eigenvectors are $|\pm\rangle = (1, \pm e^{\mp i\theta})^{\top}$, with $\sin \theta = \tilde{\Gamma}$. These eigenvectors are linearly independent and orthogonal, $\langle + | - \rangle = 0$.

Exceptional point when $|\tilde{\Gamma}| = 1$. Here occurs the transition between the unbroken and broken regimes. Both eigenvalues and their corresponding eigenvectors coalesce [116], *i. e.*, $m_{\pm} = 0$ and $|\pm\rangle = (1, i)^{\top}$. Then, a behaviour with a power law is expected.

Broken \mathcal{PT} -symmetry when $|\tilde{\Gamma}| > 1$. An exponential behaviour is expected. The eigenvalues, m_{\pm} , are imaginary numbers and its correspondent eigenvectors are $|\pm\rangle = (1, i e^{\pm\theta})^{\top}$ with $\cosh \theta = \tilde{\Gamma}$. These vectors are linearly independent but the orthogonality does not longer hold, $\langle + | - \rangle \neq 0$.

In all these regimes, the total intensity is not conserved along propagation, a feature of nonunitary evolution [117].

Chapter 3

Robust quantum-state transfer

This chapter demonstrates the possibility of a robust quantum-state transfer in an optomechanical system using a composite phase sequence [100–102], while taking into account the losses of the system. First, we review quantum-state exchange using the formalism of quantum Langevin equations for the linearized optomechanical effective model, Sec. 2.1.2. These equations are similar to those describing a qubit driven by an external coherent electromagnetic field. This similarity allows quantum-state transfer in the optomechanical system. Such transfer is sensitive to systematic errors like inaccuracies in the field magnitude, laser frequency, driving duration, coupling strength and others. Composite pulse sequences in a qubit can overcome such systematic errors and produce a robust population transfer [104]. A similar effect yields quantum-state transfer in an optomechanical system due to the connection in its QLEs. Finally, we consider the effects on the optomechanical steady-state amplitudes due to smoothness of the driving phase-sequence.

3.1 Quantum excitation exchange

We consider an optomechanical system with strong laser driving in order to use the red-detuned regime where the effective Hamiltonian leads to a beam-splitter-like interaction, $e^{i\varphi}\hat{c}^\dagger\hat{d} + e^{-i\varphi}\hat{c}\hat{d}^\dagger$, see Sec. 1.2.1. Also, we use the QLEs for quantum fluctuations operators in order to study its lossy dynamics. In a matrix form, those equations are, Sec. 2.1.2,

$$\frac{d}{dt} \begin{pmatrix} \hat{c} \\ \hat{d} \end{pmatrix} = - \begin{pmatrix} \kappa/2 + i\omega_m & ig e^{i\varphi} \\ ig e^{-i\varphi} & \gamma/2 + i\omega_m \end{pmatrix} \begin{pmatrix} \hat{c} \\ \hat{d} \end{pmatrix} - \begin{pmatrix} \sqrt{\kappa} \hat{\xi}_c \\ \sqrt{\gamma} \hat{\xi}_m \end{pmatrix}. \quad (3.1)$$

Here, we consider the cavity (mechanical) input field as Gaussian quantum noise described by the operator $\hat{\xi}_c$ ($\hat{\xi}_m$) with correlation functions,

$$\langle \hat{\xi}_{(c,m)}^\dagger(t) \hat{\xi}_{(c,m)}(s) \rangle = n_{th}^{(c,m)} \delta(t-s), \quad (3.2a)$$

$$\langle \hat{\xi}_{(c,m)}(t) \hat{\xi}_{(c,m)}^\dagger(s) \rangle = (n_{th}^{(c,m)} + 1) \delta(t-s), \quad (3.2b)$$

where $n_{th}^{(c,m)}$ is the average thermal occupation number of the baths.

To arrange the coupled QLEs, we define the constants $\Gamma = (\kappa - \gamma)/(4g)$, $\mu = (\kappa + \gamma)/4$ and the vectors $\vec{r}(t) = e^{(\mu+i\omega_m)t} \left(\hat{c}, \hat{d} \right)^\top$, $\vec{r}_{in}(t) = e^{(\mu+i\omega_m)t} \left(\sqrt{\kappa} \hat{\xi}_c, \sqrt{\gamma} \hat{\xi}_m \right)^\top$, to write,

$$-\frac{d}{dt} \vec{r}(t) = i g \hat{\mathcal{H}} \vec{r}(t) + \vec{r}_{in}(t), \quad (3.3)$$

where $\hat{\mathcal{H}}$ is a 2×2 non-Hermitian matrix,

$$\hat{\mathcal{H}} = (e^{i\varphi} \hat{\sigma}_+ + e^{-i\varphi} \hat{\sigma}_-) - i \Gamma \hat{\sigma}_z, \quad (3.4)$$

and we used the standard definition for the Pauli matrices. Up to this point, we considered the driving-laser phase, φ , as a constant value. Then, the solution for the vector $\vec{r}(t)$ is,

$$\vec{r}(t) = \hat{U}_\varphi(t - t_0) \vec{r}(t_0) - \int_{t_0}^t \hat{U}_\varphi(t - y) \vec{r}_{in}(y) dy, \quad (3.5)$$

where $t_0 < t$ is an initial time and \hat{U}_φ is the constant-phase evolution operator with matrix form given by,

$$\hat{U}_\varphi(\tau) = e^{-ig\hat{\mathcal{H}}\tau} = \cos(\Omega g \tau) \mathbb{1}_2 - \frac{i}{\Omega} \sin(\Omega g \tau) \hat{\mathcal{H}}. \quad (3.6)$$

Here, we used the notation $\mathbb{1}_2$ for the 2×2 identity matrix and introduced an effective Rabi frequency $\Omega = \sqrt{1 - \Gamma^2}$ which is a real number when the decay rates are small compared with the enhanced optomechanical coupling, $(\kappa - \gamma) \ll g$. From the arguments of the trigonometric functions of the constant-phase evolution operator, we define the time scale $\tau_0 = \pi/(2g\Omega)$ and the interaction area $A(\tau) = \Omega g \tau$. In consequence, τ_0 corresponds to $A(\tau_0) = \pi/2$ which, in the lossless case, produces complete quantum-state exchange.

Using the evolution of vector $\vec{r}(t)$, we calculate the mean photon and phonon numbers for a constant phase driving,

$$\langle \hat{c}^\dagger \hat{c} \rangle(\tau) = (n_0 |U_{11}(\tau)|^2 + m_0 |U_{12}(\tau)|^2) e^{-2\mu\tau} + \kappa n_{th}^{(c)} S_{11}(\tau) + \gamma n_{th}^{(m)} S_{12}(\tau), \quad (3.7a)$$

$$\langle \hat{d}^\dagger \hat{d} \rangle(\tau) = (n_0 |U_{21}(\tau)|^2 + m_0 |U_{22}(\tau)|^2) e^{-2\mu\tau} + \kappa n_{th}^{(c)} S_{21}(\tau) + \gamma n_{th}^{(m)} S_{22}(\tau), \quad (3.7b)$$

where the initial photon and phonon occupation numbers are n_0 and m_0 , respectively. We use the short-hand notation for the matrix elements of the evolution operator $U_{jk}(\tau) = \left[\hat{U}_\varphi(\tau) \right]_{jk}$ and we define the functions $S_{jk}(\tau) = \int_0^\tau |U_{jk}(x)|^2 e^{-2\mu x} dx$ which arise from the quantum noise correlations.

Because $U_{jk}(\tau)$ are trigonometric functions of time τ , we expect an oscillatory behaviour of the mean photon and phonon numbers. Figure 3.1(a) shows the oscillatory quantum excitation exchange between the cavity and mechanical modes under continuous power and phase driving. Figure 3.1(b) shows a density plot of the mean phonon number as function of the time and deviations from ideal interaction area $A = A(\tau_0) + \delta A$ required for a quantum excitation exchange. We used experimental values for the parameters from Ref. [79]: $g_0/\omega_m = 18.87 \times 10^{-6}$, $\kappa/\omega_m = 10.15 \times 10^{-3}$, $\gamma/\omega_m = 9.434 \times 10^{-6}$, $n_p = 180 \times 10^3$, $n_0 = 0.02$ and $m_0 = 23.25$. The bath temperature is $T = 25$ mK which is equivalent to $n_{th}^{(m)} \approx 23.25$ thermal phonons and a negligible number of thermal photons. However, the strong laser

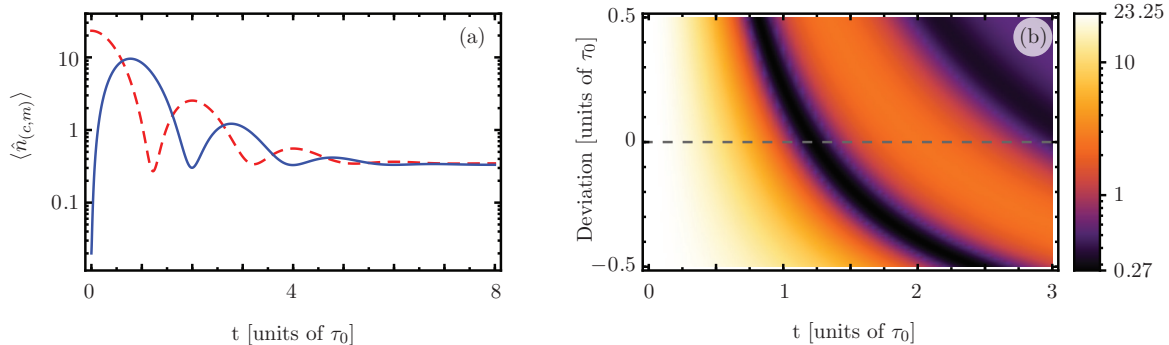


Figure 3.1: Time evolution of (a) the expectation values for the quantum photon (solid blue) and phonon (dashed red) numbers and (b) quantum expectation value for the phonon number considering deviations from the ideal accumulated interaction area, $A(\tau_0) = \pi/2$ (gray dashed line).

driving causes the cavity mode to reach a thermal equilibrium at a higher occupancy number $n_{th}^{(c)} \approx 0.305$. In this work, we assume that deviations in the interaction area arise due to variations on the laser-power. Such deviations alter the semiclassical photon number, n_p , and in consequence, the enhanced optomechanical coupling, g , changes. Also, from Figure 3.1(b), we see how the deviation from the ideal area causes a shorter or larger oscillation period when $\delta A > 0$ and $\delta A < 0$, respectively. This reveals the sensitivity to a small change due to systematic errors like laser-power.

3.2 Phase-sequence for a robust quantum excitation exchange

There is a similarity between the QLEs for the linearized optomechanical system, Eq. (3.4), and the equations that describe the complex amplitudes probabilities of a qubit driven by an external coherent electromagnetic field, Eq. (2.42). In consequence, the optomechanical system displays Rabi-like oscillations between cavity and mechanical excitations. There, some quantum control techniques can be applied to the optomechanical system. As mentioned in the previous paragraph, that characteristic leads to an inaccurate state preparation due to the sensitivity to systematic errors like laser-power, frequency, pulse duration, and others. For a qubit, a common option to produce population transfer is to use a pulse with smooth shape and defined time duration [96]. In order to improve the efficiency and robustness of the population transfer, the single pulse is replaced with a sequence of identical pulses, but the relative phase between each pulse is chosen in a way that the target state is optimized. Then, the phases of the single pulses in the sequence are the control parameter. Such technique has been well studied for a lossless qubit, Sec. 2.3, and demonstrated experimentally [104]. Here, we use the same idea to achieve a robust quantum-state transfer between the cavity and mechanical modes of the optomechanical system with losses.

We assume a phase-tailored composite pulse sequence with constant driving amplitude. Each constituent pulse in the sequence has a constant phase and a time duration correspond-

ing to an interaction area of $\pi/2$. The technique also requires an odd number of pulses such that the phases of initial and final pulse are the same. The shortest possible sequence has three pulses with total interaction area of $3\pi/2$, in consequence, the only free parameter for the control is the phase of the middle pulse. We denoted it with the Greek letter φ . Under those conditions, the final state of the system at $3\tau_0$ is given by the vector,

$$\begin{aligned} \vec{r}(3\tau_0) = & \hat{U}^{(3)}(\tau_0) \vec{r}(0) - \int_0^{\tau_0} \hat{U}^{(3)}(\tau_0) \hat{U}_0(-z) \vec{r}_{in}(z) dz \\ & - \int_{\tau_0}^{2\tau_0} \hat{U}_0(\tau_0) \hat{U}_\varphi(2\tau_0 - z) \vec{r}_{in}(z) dz - \int_{2\tau_0}^{3\tau_0} \hat{U}_\varphi(3\tau_0 - z) \vec{r}_{in}(z) dz, \end{aligned} \quad (3.8)$$

where the evolution operator $\hat{U}^{(3)} = \hat{U}_0(\tau_0) \hat{U}_\varphi(\tau_0) \hat{U}_0(\tau_0)$ is for the three-interaction composite sequence. Each operator \hat{U} describes the evolution of the optomechanical system under different driving phases. The product gives as result that each $\hat{U}_{jk}^{(3)}$ contains the phase, φ , which will produce interference. We exploit this effect to obtain robust quantum-state transfer.

We calculate the mean photon and phonon numbers with the vector $\vec{r}(3\tau_0)$. Both quantities can be split in two contributions, one is the damped oscillatory part and the other is due to the thermal noise,

$$\langle \hat{c}^\dagger \hat{c} \rangle(3\tau_0) = n_{osc}^{(c)}(3\tau_0) + n_{noise}^{(c)}(3\tau_0), \quad (3.9a)$$

$$\langle \hat{d}^\dagger \hat{d} \rangle(3\tau_0) = n_{osc}^{(m)}(3\tau_0) + n_{noise}^{(m)}(3\tau_0). \quad (3.9b)$$

The oscillatory part is analogous to the Rabi oscillations of a qubit. It is responsible for the excitation exchange between the cavity and the mechanical mode. As we discuss below, to optimize the exchange, it is enough if we work with the oscillatory part of the phonons,

$$n_{osc}^{(m)}(3\tau_0) = \left[n_0 \left| U_{21}^{(3)}(\tau_0) \right|^2 + m_0 \left| U_{22}^{(3)}(\tau_0) \right|^2 \right] e^{-6\mu\tau_0}, \quad (3.10)$$

where the matrix elements of $\hat{U}^{(3)}(\tau_0)$ are,

$$U_{11}^{(3)}(\tau_0) = [U_{11}(\tau_0)]^3 + U_{12}(\tau_0) U_{21}(\tau_0) [U_{22}(\tau_0) + 2U_{11}(\tau_0) \cos(\varphi)], \quad (3.11a)$$

$$U_{12}^{(3)}(\tau_0) = U_{12}(\tau_0) \{ [U_{11}(\tau_0)]^2 + [U_{22}(\tau_0)]^2 + e^{-i\varphi} U_{12}(\tau_0) U_{21}(\tau_0) + e^{i\varphi} U_{11}(\tau_0) U_{22}(\tau_0) \}, \quad (3.11b)$$

$$U_{21}^{(3)}(\tau_0) = U_{21}(\tau_0) \{ [U_{11}(\tau_0)]^2 + [U_{22}(\tau_0)]^2 + e^{i\varphi} U_{12}(\tau_0) U_{21}(\tau_0) + e^{-i\varphi} U_{11}(\tau_0) U_{22}(\tau_0) \}, \quad (3.11c)$$

$$U_{22}^{(3)}(\tau_0) = [U_{22}(\tau_0)]^3 + U_{12}(\tau_0) U_{21}(\tau_0) [U_{11}(\tau_0) + 2U_{22}(\tau_0) \cos(\varphi)]. \quad (3.11d)$$

Here, we used the matrix elements of $\hat{U}_0(\tau_0)$. The part due to quantum noise has a more complicated expression and is not relevant in this analysis. This is because, in our case, we are considering a high semiclassical photon number, n_p , enough to have many oscillations before the thermal contribution becomes important.

3.2. Phase-sequence for a robust quantum excitation exchange

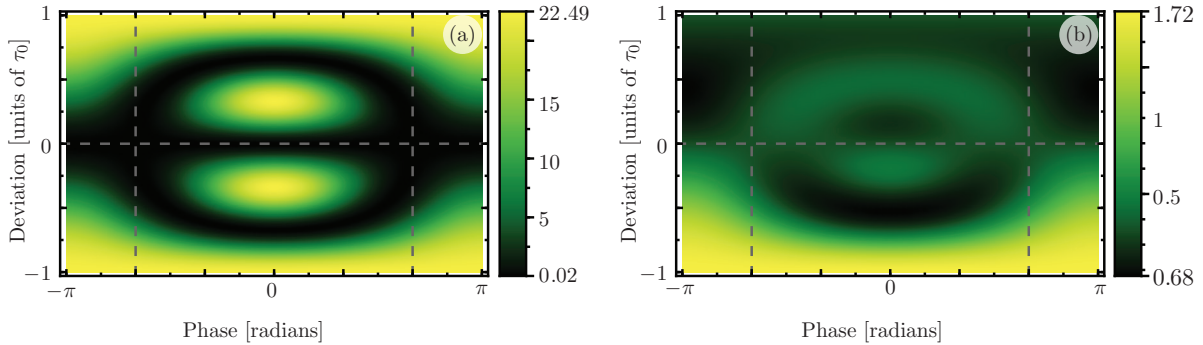


Figure 3.2: (a) Oscillatory and (b) thermal noise contributions to the phonon number as a function of deviations in the interaction area and the phase value at time $t_f = 3\tau_0$ for parameter values: $g_0/\omega_m = 1.51 \times 10^{-4}$, $\kappa/\omega_m = 145.9 \times 10^{-3}$, $\gamma/\omega_m = 5.36 \times 10^{-4}$, $n_p = 90 \times 10^3$, $(n_0, m_0) = (0.02, 23.25)$ and $n_{th}^{(c,m)} = (0.21, 32)$, taken from Ref. [97].

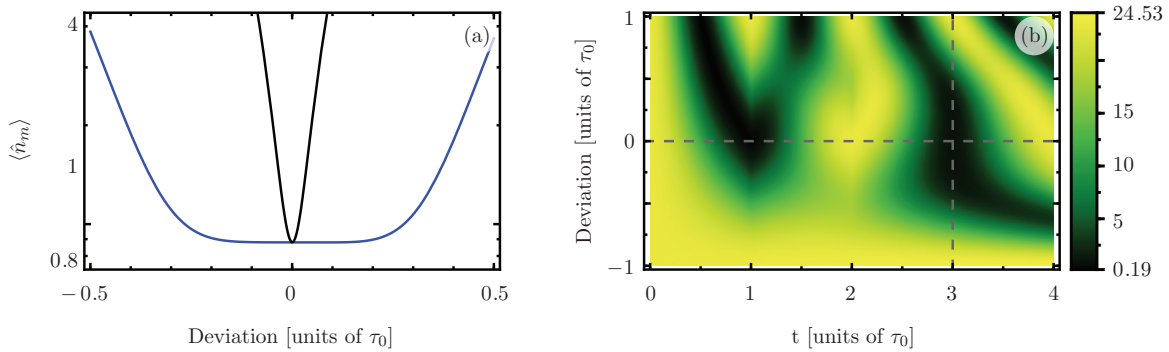


Figure 3.3: (a) Phonon number, $\langle \hat{n}_m \rangle$, after the composite sequence for driving phases $\varphi = 0$ (black), $\varphi = \pm 2\pi/3$ (blue). (b) Time evolution of the mean phonon number as a function of the deviation from ideal parameters with a driving phase $\varphi = 2\pi/3$. The optimal phases $\varphi_{opt} = \pm 2\pi/3$ are signaled by vertical dashed lines. Parameter values are equal to those in Fig. 3.2.

To achieve optimal excitation exchange, we need to minimize the component $|U_{22}^{(3)}(\tau_0)|^2$ around the single-interaction area $\pi/2$, or, alternatively, maximize $|U_{21}^{(3)}(\tau_0)|^2$. By minimizing the derivative of $|U_{22}^{(3)}(\tau_0)|^2$ with respect to the interaction area, we obtain the condition for the optimal phase,

$$\cos(\varphi_{opt}) = \frac{3\Gamma^2 - 1}{2}, \quad (3.12)$$

which for the lossless system yields $\varphi_{opt} = \pm 2\pi/3$. This is consistent with the result reported in Tab. 2.1 for a coherently-driven qubit on resonance and without losses.

In Fig. 3.2 we show density plots of the oscillatory and thermal noise contributions considering deviations in the interaction area and the phase value $-\pi < \varphi < \pi$ to illustrate the interference-like effect obtained with the phase sequence. With experimental values

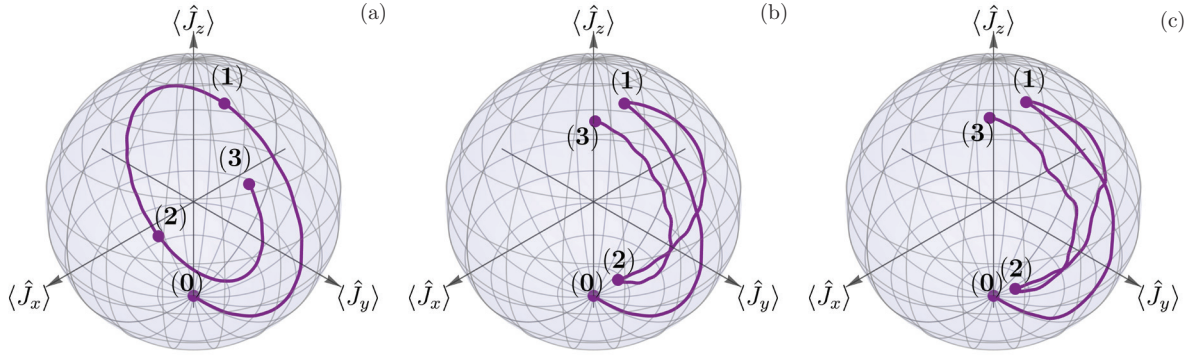


Figure 3.4: Angular momentum representation of optomechanical quantum-state transfer. (a) Displays a three-interaction evolution with a -10% deviation and constant driving phase. (b) Displays the same evolution under a composite driving sequence that maximizes robustness. (c) Displays the same evolution as (b), but where additional time-dependent white-noise fluctuations are added on the parameters g , ω_m , Δ , κ , and γ .

from Ref. [97], the optimal phase is almost identical to the lossless one, $\varphi \approx \pm 2\pi/3$, within $10^{-3}\%$. The vertical dashed lines indicate the phase value where the optimal robust excitation exchange is produced. In Fig. 3.3(a) we plotted the mean phonon number at $t_f = 3\tau_0$ with and without the phase sequence. There, we observe the robustness obtained around the total interaction area of $\delta A = 0$. In Fig. 3.3(b), like Fig. 3.1(b), we show the full time evolution for the mean phonon number under the optimal composite sequence considering deviations in the interaction area. We notice how the interference-like effect changes the behaviour of the mean phonon number when there are deviations in the interaction area, producing a region with robust quantum-state transfer near the intersection of the dashed lines.

3.2.1 Angular momentum representation and statistical analysis

In order to have visual cues, physical insight, and show that the derived optimal phase sequence produces robust quantum-state transfer, we numerically calculate the evolution using the red-detuned linearized optomechanical system under Lindblad's approach, Sec. 2.2. We display the results using the Bloch sphere for the Schwinger's two-boson representation of angular momentum [118],

$$\hat{J}_x = \frac{1}{2} (\hat{c}^\dagger \hat{d} + \hat{d}^\dagger \hat{c}), \quad (3.13a)$$

$$\hat{J}_y = \frac{-i}{2} (\hat{c}^\dagger \hat{d} - \hat{d}^\dagger \hat{c}), \quad (3.13b)$$

$$\hat{J}_z = \frac{1}{2} (\hat{c}^\dagger \hat{c} - \hat{d}^\dagger \hat{d}). \quad (3.13c)$$

In Fig. 3.4 we present three cases for the time evolution of the optomechanical quantum-state transfer for a three-interaction sequence. Initially, the cavity is at the vacuum state and the mechanical oscillator has a single quanta; also, each single-pulse has a -10% deviation from the ideal value of $\pi/2$. The first case, Fig. 3.4(a), the evolution is under constant

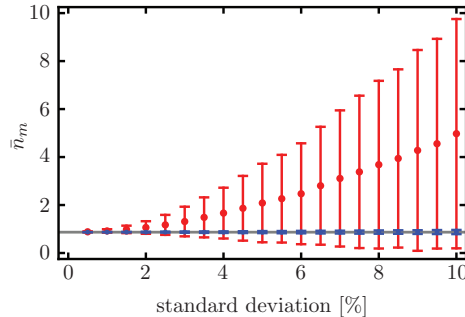


Figure 3.5: Mean value (dots) and standard deviation (bars) of samples of phonon number expectation value samples after three interactions, \bar{n}_m . Again, each of the physical parameters, g, κ, γ , is generated using a normal distribution with standard deviation determined as a percentage of the central value of the corresponding parameter. Red points and bars correspond to constant-phase evolution and blue points and bars correspond to evolution under composite phase driving. Here, the experimental values are the same as those in Fig. 3.1 and Lecocq *et al.* [79]. We used a sample consisting of 5000 instances for each point.

phase-driving. In the second case, Fig. 3.4(b), the phase-driving has a piecewise structure with the optimal phase value given by Eq. (3.12). The third case, Fig. 3.4(c), besides to the piecewise phase-driving, some parameters of the system have time-dependent white noise as an additional source of errors. In all the cases, the initial point in the Bloch sphere is labelled by (0), the successive (1), (2) and (3) points the end of each part of the three-interaction sequence. The position of final point, (3), is different for each case. In the first, we observe an incomplete quantum-state transfer due to the deviation in the single-pulse area. For the second and third cases, with the piecewise phase-driving, the quantum-state transfer is much better even in the presence of losses and, in the last case, even in presence of white noise, as mentioned before. For the last case, we generate a sequence of 50 random numbers in the range of 0.95 to 1.05 for each of the parameters. Then, that sequence is used to generate a smooth interpolated function that multiplies the baseline value of each parameter. As we can see, even in the presence of the area deviation, time-dependent random noise in the parameters of the system and time evolution under Lindblad master equation, a robust state transfer can be achieved using the composite phase sequence. The baseline values of the parameters are $g/\omega_m = 5 \times 10^{-2}$, $\kappa/\omega_m = 4 \times 10^{-3}$, $\gamma/\omega_m = 8 \times 10^{-3}$, $n_{th}^{(c,m)} = 0$ and $\Delta = -\omega_m$.

In addition, we perform a central-limit statistical analysis to validate whether or not our composite phase driving proposal produces robust optomechanical state transfer under random variations in its physical parameters. In the following, the mean values and standard deviations are calculated from the resulting quantum mean phonon value samples and do not correspond to the quantum average mean phonon number and its uncertainty. For our analysis, we calculate a large sample of simultaneous random variations on the physical parameters g, κ, γ , each of them under a normal distribution with fixed mean and standard deviation. Next, we calculate the phonon number expectation value after three interactions, $\langle \hat{n}_m(3\tau_0) \rangle$, for each of these sets. We use two scenarios: evolution under the standard red-sideband state transfer and our composite phase driving proposal. While the parameters

	Cohen <i>et al.</i> [97]		Lecocq <i>et al.</i> [79]		Gröblacher <i>et al.</i> [75]	
	Constant	Composite	Constant	Composite	Constant	Composite
central values (no random variation)						
$\langle \hat{n}_m \rangle$	0.871	0.870	0.337	0.627	0.0454	0.0456
1% σ in random variations in g, κ, γ						
\bar{n}_m	0.917	0.870	0.340	0.627	0.0950	0.0456
σ	0.0665	0.00845	0.0305	0.0128	0.0705	0.000323
2% σ in random variations in g, κ, γ						
\bar{n}_m	1.06	0.870	0.346	0.629	0.247	0.0456
σ	0.274	0.0173	0.0614	0.0263	0.289	0.000653
5% σ in random variations in g, κ, γ						
\bar{n}_m	2.06	0.871	0.385	0.638	1.20	0.0456
σ	1.592	0.0420	0.1474	0.0718	1.481	0.00164

Table 3.1: Mean value, \bar{n}_m , and standard deviation, σ , of phonon number expectation value samples resulting from randomly-variated parameters g , κ , and γ . We use three sets of central values, Cohen *et al.* [97], with $g/\omega_m = 4.62 \times 10^{-2}$, $\kappa/\omega_m = 145.9 \times 10^{-3}$, $\gamma/\omega_m = 5.36 \times 10^{-4}$; Lecocq *et al.* [79], with $g/\omega_m = 8.01 \times 10^{-3}$, $\kappa/\omega_m = 10.15 \times 10^{-3}$, $\gamma/\omega_m = 9.43 \times 10^{-6}$; and Gröblacher *et al.* [75], with $g/\omega_m = 0.434$, $\kappa/\omega_m = 227 \times 10^{-3}$, $\gamma/\omega_m = 1.48 \times 10^{-4}$; We set the following initial values $n_0 = 0.01$, $m_0 = 23.25$, $n_{th}^{(c)} = 0.21$, $n_{th}^{(m)} = 32.0$ and use 3000 instances in each sample.

g , κ , γ have random variations, the driving sequence is determined by the central values that characterize the system and, therefore, it is constant and does not suffer from random variations. Table 3.1 collects the mean value of the phonon number and its standard deviation for samples calculated with experimental parameters reported in the literature. We find that composite driving produces samples that are more robust against Gaussian deviations in their physical parameters, *i. e.*, the standard deviation of the sample of phonon numbers is much smaller under our custom phase sequence than under constant-phase driving. Also, the mean phonon number is centered around a minimum, which means that random variations are more likely to produce an increase in the average phonon number than a decrease. Table 3.1 and Fig. 3.5 show that, as the standard deviation for the random variation of the physical parameters g , κ , γ increases, the average phonon number increases and this increment is more dramatic under constant-phase driving.

3.2.2 Longer composite sequences

The composite sequence technique described above can be extended to longer number of parts with more than three interactions. Like in Sec. 2.3, we focus on sequences with an odd number of interactions, N , and were there the sequence has reversal symmetry, *i. e.*, the k -th phase obey $\phi_k = \phi_{N+1-k}$. Without loss of generality, we set $\phi_1 = \phi_N = 0$, because the quantum-state transfer is sensitive to phase changes with respect to a baseline value. Then we have $(N - 1)/2$ free phase parameters for control. Like in the three-interaction case, the evolution under that sequence can be calculated by composing the evolution vector, Eq.

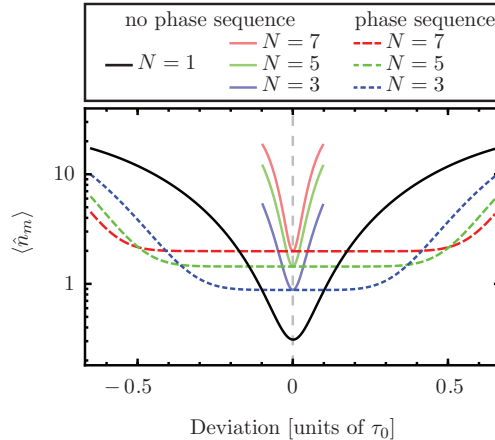


Figure 3.6: Phonon number expectation value after $N = 1, 3, 5, 7$ interactions as a function of the deviation from the ideal interaction area. Solid curves show the phonon number when the driving phase is kept constant throughout the evolution. Dashed curves show the phonon number with a nontrivial phase sequence that minimizes the effect of deviations. In this low-loss scenario we use the driving phases from the lossless case. Physical parameters have the same values as in Fig. 3.2.

(3.5), N -times to obtain, at $t_f = N \tau_0$,

$$\vec{r}(t_f) = \hat{U}^{(N)}(t_f) \vec{r}_0 - \vec{R}_{in}(t_f), \quad (3.14)$$

where \vec{R}_{in} involves integrals with the quantum noise operators, useless for our analysis. The composed evolution operator is given by,

$$\hat{U}^{(N)}(N \tau_0) = \hat{U}_{\phi_1}(\tau_0) \hat{U}_{\phi_2}(\tau_0) \cdots \hat{U}_{\phi_2}(\tau_0) \hat{U}_{\phi_1}(\tau_0). \quad (3.15)$$

Like in the three-interaction case, the photon and phonon numbers can be written as the sum of two contributions, the damped oscillatory part and the thermal noise part. To obtain a robust excitation transfer, we nullify the first $(N - 1)/2$ derivatives of $|U_{22}^{(N)}|^2$ with respect to the single-pulse interaction area of $\pi/2$. From that procedure we obtain a system of $(N - 1)/2$ coupled non-linear equations for the $(N - 1)/2$ optimal phases which can be solved numerically. In the lossless case, the analytical phase values are given by Eq. (2.49). In the case when $\Gamma \approx 0$, the optimal phases are quite similar to those of the lossless case. This produces a more robust optomechanical excitation exchange by increasing the region of parameters where the phonon number is stable against deviations, see Fig. 3.6. A trade-off of long composite sequences is that decoherence plays a more important role. Therefore, in high-loss scenarios, long driving sequences should be avoided.

3.3 Smooth phase-sequence

In the previous section we considered the phase-driving as a piecewise function which takes constant values in each interval of time $t_k - t_{k-1} = \tau_0$ and discontinuous at the times $k \tau_0$, with

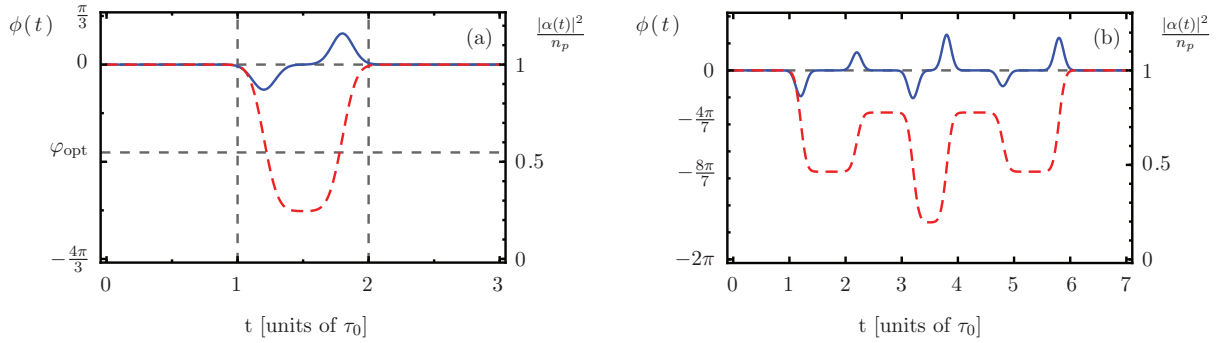


Figure 3.7: (a) Three- and (b) seven-interaction smooth phase-sequences, $\phi(t)$ (red dashed curve), and normalized semiclassical field intensity, $|\alpha(t)|^2/n_p$ (blue solid curve). For both (a) and (b), the scale on the left vertical axis corresponds to the phase sequence and the scale on the right vertical axis corresponds to the normalized intensity.

$k = 1, \dots, N - 1$. That jump in the phase value causes abrupt changes in the steady-state amplitude values of the optomechanical system, α and β . To make such effect less significant, we consider the phase-driving like a smooth function of time which resembles the piecewise version. Then, α and β change smoothly over time and return to their steady-state values. Also, changes in the detuning Δ and the single-interaction area can be negligible.

To exemplify this assertion, we numerically solved the time evolution of α and β when the phase-driving is a smooth function for the three-interaction case. The differential equations and the explicit form of the phase are,

$$\frac{d\alpha}{dt} = -\left(\frac{\kappa}{4} + i\omega_m\right)\alpha + \frac{ie^{-i\phi}\varepsilon}{2}, \quad (3.16a)$$

$$\frac{d\beta}{dt} = -\left(\frac{\gamma}{4} + i\omega_m\right)\beta - ig_0|\alpha|^2, \quad (3.16b)$$

$$\phi(t) = \varphi_{\text{opt}} f \theta_s [t - (1.2)\tau_0, \sigma] \theta_s [(1.8)\tau_0 - t, \sigma], \quad (3.16c)$$

where the smooth phase is based on the error function, $\theta_s(x, \sigma) = [\text{erf}(x/\sigma) + 1]/2$. We introduced two parameters, $\sigma = \tau_0/25$ and f . The former controls the smoothness of the pulse and the latter is a dimensionless value that keeps the average of the phase at its optimal value, $\varphi_{\text{opt}} = 2\pi/3$. In this case, the average phase value in the interval $[\tau_0, 2\tau_0]$ is approximately -1.89 rad; we used the negative value for the simulations. Then, the semiclassical amplitudes α and β smoothly change a percentage from its steady-state value. The semiclassical EM field amplitude changes within 8%. This leads to less than a 0.2% of difference in the three-interaction area and keeps the detuning, Δ , within 0.005% of its value. In Fig. 3.7(a) we display the smooth phase function with the time evolution of the semiclassical number of photons in the cavity, $|\alpha(t)|^2/n_p$, for the three-interaction sequence. We notice the changes of $\alpha(t)$ around the times τ_0 and $2\tau_0$ where the phase-driving increases or decreases smoothly. In Fig. 3.7(b), we numerically calculated the effect of a seven-interaction sequence with a similar procedure like before, using the phase values $\{0, -6\pi/7, -4\pi/7, -8\pi/7, -4\pi/7, -6\pi/7, 0\}$ given for the lossless case which are almost identical for the experimental parameters considered. Under this sequence, the semiclassical number of photons remains within 10% of

its steady-state value and keeps the total interaction area within 0.1% of the ideal value of $7\pi/2$. Also, after each phase-driving sequence, the semiclassical amplitude $\alpha(t)$ returns to its steady-state value as can be observed in both examples. This seems natural because the phase value of α returns to its constant initial value after the complete interaction.

3.4 Conclusions

We reviewed the quantum-state swap in optomechanical systems under the red-detuned regime and constant laser-power. We observed that such process is very sensitive to systematic errors, specially those inherit by the laser-power errors, Fig. 3.1(b). Then, the implementation of phase-driving through the laser produces robustness against systematic errors. This is analogous to the BB composite sequence developed for a lossless qubit, Sec. 2.3. We present analytical results for a three-part sequence in the optomechanical system, Fig. 3.3. The lossy dynamics considered in this work produces a slightly different optimal phase value for robust quantum excitation exchange, Eq. (3.12). Considering a larger enhanced optomechanical coupling compared with the damping rates, allows us to use the phase-driving values showed in Table 2.1. Then, we perform purely numerical simulations for the three-part sequence using Lindblad master equation. We observed the robustness in quantum-state transfer even in the presence of white noise in some of the optomechanical parameters, Fig. 3.4. After that, we showed how the increasing number of parts in the phase-driving produces a more robust quantum excitation exchange, Fig. 3.6. Finally, we studied numerically the effects on the semiclassical amplitudes due to smooth phase-driving, Fig. 3.7. The changes on the interaction area and detuning due to the smooth shape of the phase-driving are negligible. In consequence, the smooth approximation to the piecewise phase-sequence produces a similar robust quantum-state transfer. All this results are published in Ref. [119], see Appendix A.

Chapter 4

Non-Hermitian optomechanics

This chapter deals with lossy optomechanical system with red-detuning. Here, we link its strong and weak coupling regimes with an effective non-Hermitian dynamics that can be selected using the laser' power. First we briefly review the optomechanical coupling regimes which are based on the nature of the red-detuned eigenfrequencies. Next, we relate those regimes to the ones of a two-waveguide coupler with \mathcal{PT} -symmetry, Sec. 2.4.1. That relation came out from the QLEs of the quantum fluctuations operators in Sec. 1.2.1. Then, we numerically compare the time evolution given by non-Hermitian Schrödinger equation with the one produced with Lindblad master equation, both at zero temperature. These two approaches show differences and similarities depending on the initial quantum-states. Finally, we used analytical expressions obtained with the QLEs for an initial mechanical thermal state at finite temperature and negligible photons in the EM field. The achievement of this last result is the clear observation of \mathcal{PT} -symmetry regimens at finite temperature.

4.1 Optomechanical eigenfrequencies

We consider an optomechanical system with strong laser driving in order to use the red-detuned regime where the effective Hamiltonian leads to a beam-splitter-like interaction, $e^{i\varphi}\hat{c}^\dagger\hat{d} + e^{-i\varphi}\hat{c}\hat{d}^\dagger$, see Sec. 1.2.1. We use the QLEs for quantum fluctuations operators in order to study its lossy dynamics, Eq. (3.1), which can be written like,

$$-\frac{d}{dt}\vec{v} = \mathcal{M}\vec{v} + \vec{v}_{in}, \quad (4.1)$$

where $\vec{v} = (\hat{c}, \hat{d})^\top$, $\vec{v}_{in} = (\sqrt{\kappa}\hat{\xi}_c, \sqrt{\gamma}\hat{\xi}_m)^\top$ and the drift matrix \mathcal{M} is,

$$\mathcal{M} = \begin{pmatrix} \kappa/2 + i\omega_m & ig \\ ig & \gamma/2 + i\omega_m \end{pmatrix}. \quad (4.2)$$

Here, we omitted the laser-phase value because it remains constant throughout this analysis. Like in Chapter 3, we are not interested in the dynamics due to the quantum noise operators. The matrix \mathcal{M} determines the optomechanical dynamics. Therefore it is important to look at its eigenfrequencies,

$$\lambda_{\pm} = \mu + i\omega_m \pm i|g|\Omega, \quad (4.3)$$

where we used the definitions of $\mu = (\kappa + \gamma)/4$, $\Gamma = (\kappa - \gamma)/(4g)$ and $\Omega = \sqrt{1 - \Gamma^2}$ given in Sec. 3.1. Because the matrix \mathcal{M} is not time-dependent, we can write the time evolution for the optomechanical operators in the form,

$$\vec{v}(t) = e^{-(\mu+i\omega_m)t} \mathcal{Q}^{-1} \text{diag} (e^{-i\Omega|g|t}, e^{i\Omega|g|t}) \mathcal{Q} \vec{v}(0) + \vec{V}_{in}(t), \quad (4.4a)$$

$$= e^{-(\mu+i\omega_m)t} \hat{U}(t) \vec{v}(0) + \vec{V}_{in}(t), \quad (4.4b)$$

where \mathcal{Q} is a 2×2 matrix whose first and second columns are the eigenvectors of $m_+ = |g|\Omega$ and $m_- = -|g|\Omega$, respectively, see Sec. 2.4.1. This eigendecomposition is valid for $m_+ \neq m_-$. Also, the vector $\vec{V}_{in}(t)$ contains all the terms due to the quantum noise operators. The compact form in Eq. (4.4b) introduces the evolution operator \hat{U} .

The time evolution given by the QLEs, Eq. (4.4b), can present oscillatory behaviour, like the one derived throughout Chapter 3, power law or exponential dynamics. It is directly related to the values of real and imaginary parts of $\Omega = \Omega(\Gamma)$. For a simplified insight we assume $\gamma \ll \kappa$, see Table 1.1. Then, those three regimes are [1, 75, 120, 121],

Strong coupling regime : for $g \gg \kappa$ we have $\text{Re}\{\Omega\} \neq 0$ and $\text{Im}\{\Omega\} = 0$. A normal mode-splitting occurs, *i. e.*, the EM and mechanical modes hybridized. This indicates an oscillatory behaviour which allows quantum-state transfer, see the correspondent analysis in Sec. 3.1. Then, the eigenfrequencies are $\lambda_{\pm} = \mu + i(\omega_m \pm |g|\Omega)$.

Transition point between the strong and weak coupling regimes is determined by the threshold value $\kappa = 4g$ for which $\lambda_+ = \lambda_-$. This transition is observed by the homodyne detection scheme of the phase spectral density in the transmitted light [121].

Weak coupling regime : for $g \ll \kappa$ we have $\text{Re}\{\Omega\} = 0$ and $\text{Im}\{\Omega\} \neq 0$. The exponential behaviour arises and there is not hybridization mode. The approximate eigenfrequencies are,

$$\lambda_+ \approx \frac{\kappa}{2} + i\omega_m, \quad (4.5a)$$

$$\lambda_- \approx \frac{\gamma}{2} + \frac{2g^2}{\kappa} + i\omega_m. \quad (4.5b)$$

The eigenfrequency λ_+ corresponds to the EM mode with damping rate $\kappa/2$. The eigenfrequency λ_- corresponds to the mechanical mode with a modified damping rate $\gamma/2 + \gamma_{opt}$. The additional quantity $\gamma_{opt} = 2g^2/\kappa$ is known as optical damping rate which is a direct consequence of the radiation pressure exerted by the driving-laser.

4.1.1 \mathcal{PT} -symmetry approach

The three optomechanical regimes described before can be seen as the well-know regimes for a two-waveguide coupler with \mathcal{PT} -symmetry, Sec. 2.4.1, with its correspondent characteristics. For more general view, in the following we consider the parameter Γ as indicator for this regimes:

Unbroken \mathcal{PT} -symmetry when $|\Gamma| < 1$. This is the optomechanical strong coupling regime.

Transition point for the threshold value $|\Gamma| = 1$. This exceptional point marks the passage between the strong and weak optomechanical coupling regimes. Then, a power law behaviour is expected in the time evolution.

Broken \mathcal{PT} -symmetry when $|\Gamma| > 1$. This is the optomechanical weak coupling regime.

The enhanced optomechanical coupling, $g = g_0 \sqrt{n_p}$, is the only parameter that is able to vary. This is possible through the laser's power which is directly related with $n_p = |\alpha_{ss}|^2$, see Eq. (2.22). Therefore, the parameter to tune between the \mathcal{PT} -symmetry regimes is the laser's power. From the threshold value $|\Gamma| = 1$, one can obtain the critical number of photons injected by the laser $n_{cri} = (\kappa - \gamma)^2 / (4g_0)^2$, above (below) this value the obtained behaviour is the unbroken (broken) regime.

The evolution operator $\hat{U}(t)$ takes different form depending on the value of $|\Gamma|$, assuming without loss of generality $g > 0$,

$$\hat{U}_{osc}(t) = \cos(\Omega g t) \mathbb{1}_2 - \frac{i}{\Omega} \sin(\Omega g t) \hat{\mathcal{H}}, \quad \text{for } |\Gamma| < 1, \quad (4.6a)$$

$$\hat{U}_{EP}(t) = \mathbb{1}_2 - i g t \hat{\mathcal{H}}, \quad \text{for } |\Gamma| = 1, \quad (4.6b)$$

$$\hat{U}_{exp}(t) = \cosh(|\Omega| g t) \mathbb{1}_2 - \frac{i}{|\Omega|} \sinh(|\Omega| g t) \hat{\mathcal{H}}, \quad \text{for } |\Gamma| > 1, \quad (4.6c)$$

where $\hat{\mathcal{H}} = \hat{\sigma}_x - i\Gamma \hat{\sigma}_z$. In these expressions it is clear the well-known behaviours of the \mathcal{PT} -symmetry regimes described in Sec. 2.4.1. Also, we have $\hat{U}_{osc} \rightarrow \hat{U}_{EP} \leftarrow \hat{U}_{exp}$ in the limit when $|\Gamma| \rightarrow 1$.

4.2 Differences in the evolutions

From the QLEs for \hat{c} and \hat{d} , we obtain the non-Hermitian Hamiltonian,

$$\hat{H}_{nH} = \hat{H}_{red} - \frac{i}{2} \left(\kappa \hat{c}^\dagger \hat{c} + \gamma \hat{d}^\dagger \hat{d} \right), \quad (4.7)$$

where $\hat{H}_{red} = \omega_m \left(\hat{c}^\dagger \hat{c} + \hat{d}^\dagger \hat{d} \right) + g \left(\hat{c}^\dagger \hat{d} + \hat{d}^\dagger \hat{c} \right)$ is the linearized Hamiltonian with red-detuning for the optomechanical fluctuations. With this non-Hermitian Hamiltonian, it is possible to recover the QLEs, *i. e.*, the part $-\partial_t \vec{v} = \mathcal{M} \vec{v}$ in Eq. (4.1) is produced with the equation $\partial_t \hat{O}_S = i \left[\hat{H}_{nH}, \hat{O}_S \right]$ for $\hat{O}_S = \hat{c}, \hat{d}$. This is equivalent to analyse the system at zero temperature. From it, we follow a non-Hermitian Schrödinger equation (NHSE),

$$i \frac{d}{dt} |\psi\rangle = \hat{H}_{nH} |\psi\rangle. \quad (4.8)$$

The Hamiltonian in this equation can be written like,

$$\hat{H}_{nH} = \hat{H}_{env} + g \left[\hat{c}^\dagger \hat{d} + \hat{d}^\dagger \hat{c} - i\Gamma \left(\hat{c}^\dagger \hat{c} - \hat{d}^\dagger \hat{d} \right) \right]. \quad (4.9)$$

We define the envelope Hamiltonian $\hat{H}_{env} = (\omega_m - i\mu) \left(\hat{c}^\dagger \hat{c} + \hat{d}^\dagger \hat{d} \right)$. So, the NHSE can be turned into the \mathcal{PT} -symmetric model for a photonic lattice showed in Ref. [117] using the

Schwinger's two-boson representation of angular momentum in Sec. 3.2.1. The nonunitary transformation for that purpose is $\hat{V}(t) = e^{-i\hat{H}_{env}t}$. Using Eq. (4.8), the \mathcal{PT} -symmetric Hamiltonian is,

$$\hat{H}_{PT} = \hat{V}^{-1}(t) \left[\hat{H}_{nH} - \hat{H}_{env} \right] \hat{V}(t), \quad (4.10a)$$

$$= g \left[\hat{c}^\dagger \hat{d} + \hat{d}^\dagger \hat{c} - i\Gamma \left(\hat{c}^\dagger \hat{c} - \hat{d}^\dagger \hat{d} \right) \right]. \quad (4.10b)$$

Here we used $|\psi\rangle = \hat{V}(t) |\psi_{PT}\rangle$ which leads to $i\partial_t |\psi_{PT}\rangle = \hat{H}_{PT} |\psi_{PT}\rangle$. Again, we obtain the parameter Γ which is used as indicator of the unbroken/broken \mathcal{PT} -symmetry.

The nonunitary transformation, $\hat{V}(t)$, resembles the exponential $e^{-(\mu+i\omega_m)t}$ which appears in the time evolution given by the QLEs, Eq. (4.4b). Interestingly, \hat{V} depends directly on the total number of excitations in the optomechanical system, $\hat{N} = \hat{c}^\dagger \hat{c} + \hat{d}^\dagger \hat{d}$. This feature makes the difference between time evolution of $\langle \hat{c}^\dagger \hat{c} \rangle$ and $\langle \hat{d}^\dagger \hat{d} \rangle$ using the NHSE or the Lindblad master equation (2.41),

$$\begin{aligned} \frac{d}{dt} \hat{\rho} = & -i \left[\hat{H}_{red}, \hat{\rho} \right] + \frac{\kappa n_{th}^{(c)}}{2} \hat{L} \left[\hat{c}^\dagger \right] \hat{\rho} + \frac{\kappa \left(n_{th}^{(c)} + 1 \right)}{2} \hat{L} \left[\hat{c} \right] \hat{\rho} \\ & + \frac{\gamma n_{th}^{(m)}}{2} \hat{L} \left[\hat{d}^\dagger \right] \hat{\rho} + \frac{\gamma \left(n_{th}^{(m)} + 1 \right)}{2} \hat{L} \left[\hat{d} \right] \hat{\rho}, \end{aligned} \quad (4.11)$$

where the average thermal excitation number is $n_{th}^{(x)} = (e^{\hbar\omega_x/(k_B T_x)} - 1)^{-1}$ and we use the definition $\hat{L}[\hat{o}] \hat{\rho} = 2\hat{o} \hat{\rho} \hat{o}^\dagger - (\hat{o}^\dagger \hat{o} \hat{\rho} + \hat{\rho} \hat{o}^\dagger \hat{o})$.

It is straightforward to obtain the equations of motion for mean excitations numbers at zero temperature, $n_{th}^{(c,m)} = 0$. In a general way, those equations follows $\partial_t \langle \hat{O}_S \rangle = \text{Tr} \left\{ \hat{O}_S \partial_t \hat{\rho} \right\}$. We take two different approaches for the time evolution of the density matrix, one is using the Lindblad master equation (4.11) or the NHSE (4.8). In the latter, $\hat{\rho}$ evolves following,

$$\partial_t \hat{\rho} = i \left(\hat{\rho} \hat{H}_{nH}^\dagger - \hat{H}_{nH} \hat{\rho} \right). \quad (4.12)$$

Then, with the Lindblad master equation at $T = 0$,

$$\frac{d}{dt} \langle \hat{c}^\dagger \hat{c} \rangle_H = 2g \text{Im} \langle \hat{c}^\dagger \hat{d} \rangle_H - \kappa \langle \hat{c}^\dagger \hat{c} \rangle_H, \quad (4.13a)$$

$$\frac{d}{dt} \langle \hat{d}^\dagger \hat{d} \rangle_H = -2g \text{Im} \langle \hat{c}^\dagger \hat{d} \rangle_H - \gamma \langle \hat{d}^\dagger \hat{d} \rangle_H, \quad (4.13b)$$

and with the NHSE,

$$\frac{d}{dt} \langle \hat{c}^\dagger \hat{c} \rangle_{nH} = 2g \text{Im} \langle \hat{c}^\dagger \hat{d} \rangle_{nH} - \kappa \langle \hat{c}^\dagger \hat{c} \hat{c}^\dagger \hat{c} \rangle_{nH} - \gamma \langle \hat{c}^\dagger \hat{c} \hat{d}^\dagger \hat{d} \rangle_{nH}, \quad (4.14a)$$

$$\frac{d}{dt} \langle \hat{d}^\dagger \hat{d} \rangle_{nH} = -2g \text{Im} \langle \hat{c}^\dagger \hat{d} \rangle_{nH} - \gamma \langle \hat{d}^\dagger \hat{d} \hat{d}^\dagger \hat{d} \rangle_{nH} - \kappa \langle \hat{c}^\dagger \hat{c} \hat{d}^\dagger \hat{d} \rangle_{nH}. \quad (4.14b)$$

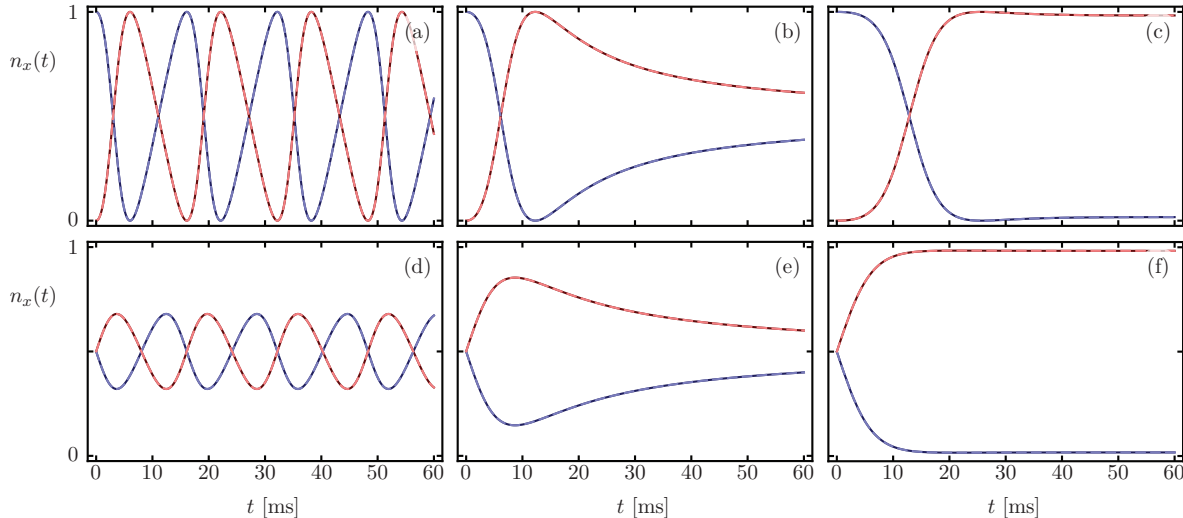


Figure 4.1: Time evolution of the instantaneously renormalized photons (blue) and phonons (red) for an initial (a-c) separable and (d-f) correlated state in the single excitation case. The solid and dashed lines corresponds to the Lindblad and NHSE evolutions, respectively. The columns show the unbroken, transition point and broken regimes, from left to right.

4.2.1 Numerical simulations

The Eqs. (4.13a), (4.13b), (4.14a), (4.14b) reveal the differences between the time evolutions produced by Lindblad master equation or NHSE. For visual cues, we numerically simulate the time evolution of the mean excitation numbers for separable and correlated initial states of the optomechanical system, $|\psi(0)\rangle = |\psi_0\rangle$. We are assuming $n_{th}^{(c,m)} = 0$ with the parameters $\omega_c = 1.02 \times 10^{10}$ Hz, $\omega_m = 1.59 \times 10^7$ Hz, $\kappa = 3.26 \times 10^5$ Hz and $\gamma = 300$ Hz. To exploit the \mathcal{PT} -symmetry regimes, we choose the critical value for the enhanced optomechanical coupling $g_{cri}/\omega_m = 5.121 \times 10^{-3}$. Then, for $g = 1.33 \times \omega_m \times 10^{-2} > g_{cri}$ we obtain the unbroken regime and for $g = 1.33 \times \omega_m \times 10^{-3} < g_{cri}$ the broken regime. To present the results, we find useful to define the instantaneously renormalized numbers,

$$n_c(t) = \frac{\langle \hat{c}^\dagger \hat{c} \rangle}{\langle \hat{N} \rangle}, \quad (4.15a)$$

$$n_m(t) = \frac{\langle \hat{d}^\dagger \hat{d} \rangle}{\langle \hat{N} \rangle}, \quad (4.15b)$$

where we are using the operator for the total number of excitations in the optomechanical system $\hat{N} = \hat{c}^\dagger \hat{c} + \hat{d}^\dagger \hat{d}$. The initial states are given in terms of the Fock basis where the first (second) entry is for the EM (mechanical) state, *i. e.*, $|k_c\rangle \otimes |k_m\rangle = |k_c, k_m\rangle$ with k_c (k_m) photons (phonons). Also, the correlated states are $N00N$ are $(|N, 0\rangle + |0, N\rangle)/\sqrt{2}$ with N an integer number.

First, we discuss the single-excitation case, $\langle \hat{N}(t=0) \rangle = 1$. For this example, the time

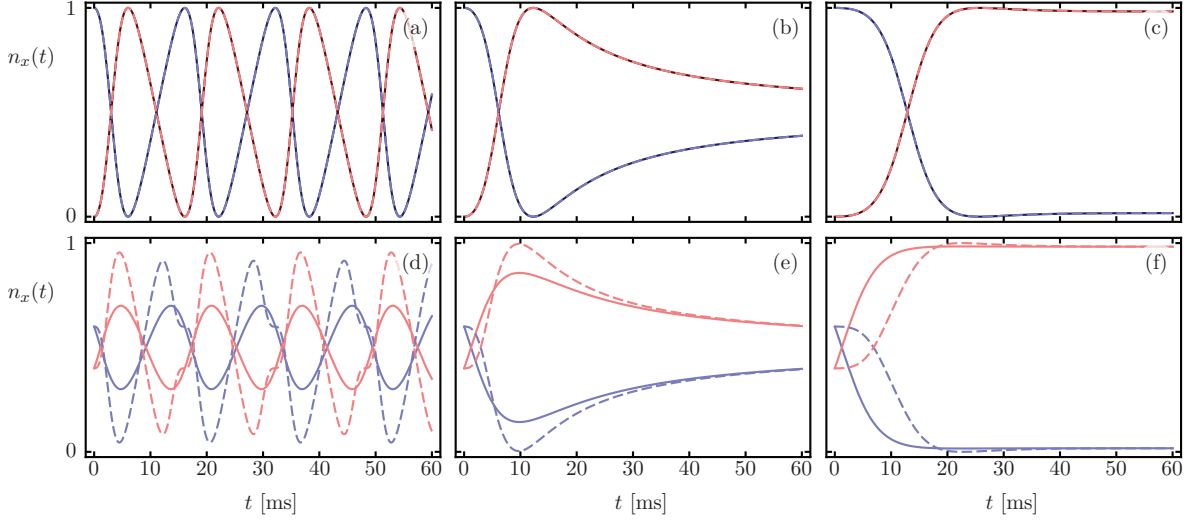


Figure 4.2: Time evolution of the instantaneously renormalized photons (blue) and phonons (red) for an initial separable state of the form (a-c) $|N, 0\rangle$ and (d-f) $|N - m, m\rangle$, with $N = 5$ and $m = 2$. The solid and dashed lines corresponds to the Lindblad and NHSE evolutions, respectively. The columns show the unbroken, transition point and broken regimes, from left to right.

evolutions are identical,

$$\frac{d}{dt} \langle \hat{c}^\dagger \hat{c} \rangle_H = \frac{d}{dt} \langle \hat{c}^\dagger \hat{c} \rangle_{nH} = 2g \operatorname{Im} \langle \hat{c}^\dagger \hat{d} \rangle - \kappa \langle \hat{c}^\dagger \hat{c} \rangle, \quad (4.16a)$$

$$\frac{d}{dt} \langle \hat{d}^\dagger \hat{d} \rangle_H = \frac{d}{dt} \langle \hat{d}^\dagger \hat{d} \rangle_{nH} = -2g \operatorname{Im} \langle \hat{c}^\dagger \hat{d} \rangle - \gamma \langle \hat{d}^\dagger \hat{d} \rangle. \quad (4.16b)$$

This result is obtained because the total number of excitations is conserved, $[\hat{N}, \hat{H}_{red}] = 0$, and when the system is open at zero temperature, the number of total excitations decays. Then, the density matrix just conserves the terms which corresponds to equal or less than one excitation. In consequence, the quadratic expectation values follows $\langle \hat{\rho}^\dagger \hat{\rho} \hat{\rho}^\dagger \hat{\rho} \rangle = \langle \hat{\rho}^\dagger \hat{\rho} \rangle$ for the single-excitation case. In Fig. 4.1 we show the numerical simulation for the instantaneous normalized photon and phonon numbers considering an initial separable state $|\psi_0\rangle = |1, 0\rangle$ and the correlated state $|\psi_0\rangle = (|1, 0\rangle + |0, 1\rangle) / \sqrt{2}$. There are not differences in the three \mathcal{PT} -symmetry regimes with both time evolution approaches, as it was expected from Eqs. (4.16).

An interesting results arises for separable states of the form $|N - m, m\rangle$ with the integer number $0 \leq m \leq N - 1$. When $m = 0$, the results produced with Lindblad master equation and NHSE are identical, see Fig. 4.2(a-c). Differences in the numerical time evolutions appear for $m > 0$, see Fig. 4.2(d-f). In the latter case, the evolutions with the NHSE show interferences, which is expected. This is because the NHSE-evolution keeps coherence and provides dissipation without preserving the state norm, while the Lindblad master equation preserves the norm of the state and provides dissipation and decoherence. Still, we observe the well defined three \mathcal{PT} -symmetry regimes. The anharmonic oscillations in the unbroken regime have a slightly different period. While in the transition point and broken regime, both

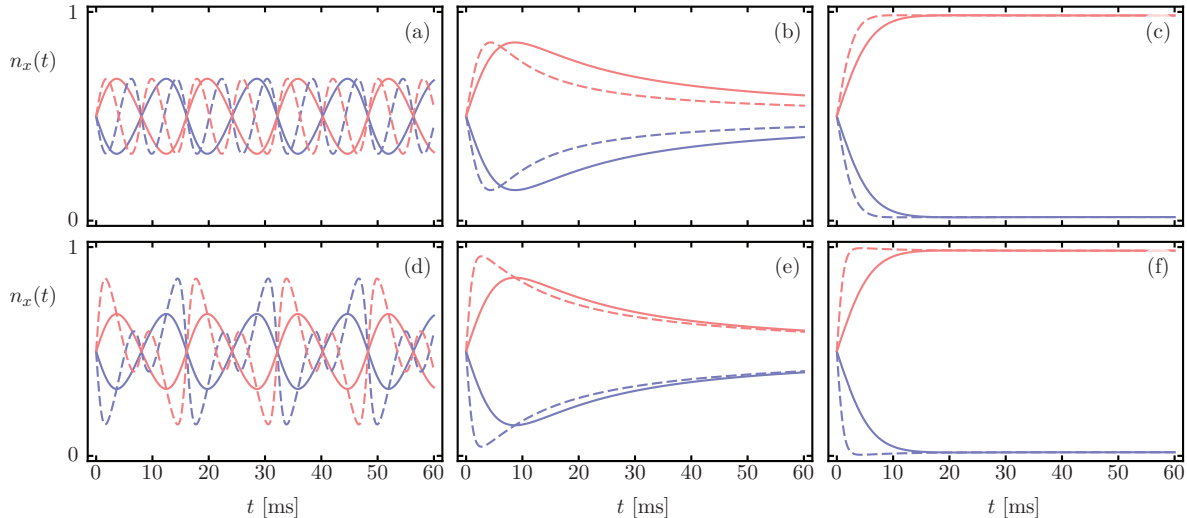


Figure 4.3: Time evolution of the instantaneously renormalized photons (blue) and phonons (red) for an initial correlated $N00N$ state with (a-c) $N = 2$ and (d-f) $N = 5$. The solid and dashed lines corresponds to the Lindblad and NHSE evolutions, respectively. The columns show the unbroken, transition point and broken regimes, from left to right.

results converge asymptotically.

In Fig. 4.3, we considered a correlated initial state $N00N$, $|\psi_0\rangle = (|N, 0\rangle + |0, N\rangle) / \sqrt{2}$. Like in the previous example, the unbroken regime shows interference for the NHSE-evolution but now the anharmonic oscillations period seems the same compared with the Lindblad's evolution. Again, in the exceptional point and broken regime, the results converge asymptotically.

For the last example, we considered the EM and mechanical states in thermal equilibrium. This assumption relies on reported experiments at finite temperature $T = 293$ K, like in Ref. [97]. For this case, we use the analytical time evolution provided by the QLEs, Eq. (4.4b), with its correspondent evolution operator, Eqs. (4.6), for each \mathcal{PT} -symmetry regime. The finite temperature produces a high thermal occupation numbers which strongly impacts in the behaviours of the photons and phonons at long times, *i. e.*, the number of the thermal excitations produced by the quantum noise increases rapidly as can be seen in Fig. 4.4(a), where the oscillations with smaller amplitude are thermal.

4.3 Conclusions

We linked the strong and weak coupling regimes of the optomechanical red-detuned system with the unbroken and broken regimes of a \mathcal{PT} -symmetric Hamiltonian, Sec. 4.1.1. In the strong and weak coupling regimes, the enhanced optomechanical parameter g serves as indicator of each regime. It is possible to exert control over optomechanical dynamics through g which is directly connected with the laser's power. Then, we numerically evolve the density matrix according a Lindblad or non-Hermitian approaches, Sec. 4.2. We choose certain values of g larger or smaller than a critical value g_{cri} to obtain the \mathcal{PT} -symmetry regime desired.

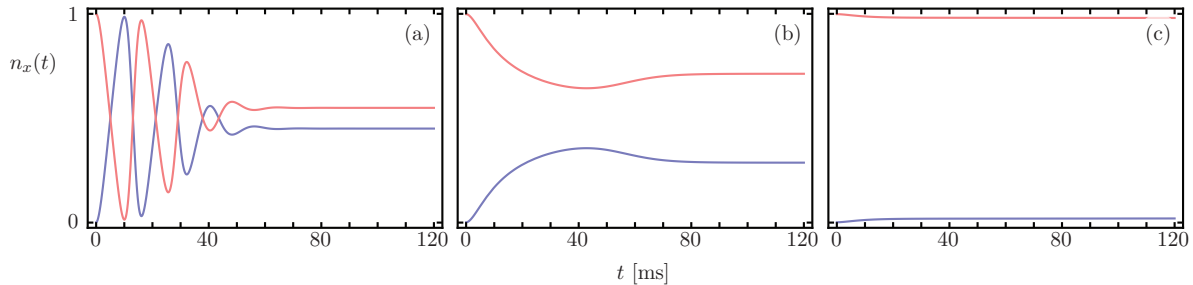


Figure 4.4: Time evolution of the instantaneously renormalized photons (blue) and phonons (red) for an initial thermal state at room temperature which is equivalent to 3, 759.68 and 2.4122×10^6 thermal photons and phonons, respectively.

Even though both approaches show some differences in the evolutions, Sec. 4.2.1, every result produced numerically shows the essential characteristics of the three regimes described in Sec. 4.1.1 and it does not matter if the initial state is or not correlated. Even more, we analytically studied the case when both modes are in thermal equilibrium, *i. e.*, both initial states are thermal and the simulations were done at room temperature. This analysis was obtained with evolution operators, Eqs. (4.6), provided by the QLEs, Eq. (4.1). In this case, we observe the influence of thermal excitations in the three regimes, Fig. 4.4.

Additionally, we showed that both approaches produces identical time evolutions at zero temperature in the single-excitation case, Fig. 4.1, and for initial separable states where one of the modes is the vacuum and the other a Fock number, Fig. 4.2(a-c). While for separable initial Fock states distinct of the vacuum, the dynamics are different, Fig. 4.2(d-f). Similar characteristics are observed for initial correlated states $N00N$, Fig. 4.3. The behaviour of the anharmonic oscillations is different using Lindblad or NHSE approaches, while in the exceptional and broken regimes both evolutions converge asymptotically. This is because the NHSE-evolution keeps coherence and provides dissipation without preserving the state norm, while the Lindblad master equation preserves the norm of the state and provides dissipation and decoherence.

Chapter 5

Conclusions

In this thesis we studied the open dynamics of an optomechanical system and two ways in which it is possible to exert control over it using the laser's phase or power, Chapter 3 and Chapter 4 respectively. The toy model we used for the results produced in the mentioned chapters is the linearized optomechanical system with red-detuning, Sec. 1.2.1. In order to analyse the open dynamics, we use quantum Langevin equations, Sec. 2.1, and Lindblad master equation, Sec. 2.2. We mainly obtain analytical results with the Langevin approach, while the Lindblad master equation was used for many numerical simulations. The optomechanical parameters used to show the benefits of our proposed techniques are within the state of art in optomechanical realizations. This makes us think that our proposed techniques for optomechanical control can be performed in current experimental realizations.

In Chapter 3 we proposed a phase-tailored sequence as control technique for robust quantum-state transfer in optomechanical systems. This technique uses the laser's phase to exert the control over the quantum excitation exchange. As realistic scenario, we considered the optomechanical system in contact with a thermal bath at finite temperature, like in Ref. [79]. The results produced show the benefits of our technique compared with the case when the sequence is not used. We started the analysis with the shortest possible sequence composed by three parts. In that case, the thermal excitation due to the finite temperature bath are negligible. Using a Bloch sphere we could visualize the quantum-state transfer with and without the phase-tailored sequence. We appreciated the favourable performance of the technique even when we added time-dependent white noise fluctuations to other parameters of the system, Fig. 3.4. Later, we extend the analysis to larger sequences where the effect of the thermal bath becomes observable. In that case, the technique still shows good results, Sec. 3.2.2, proving that our phase tailored sequence produces robustness in quantum-state exchange. Finally, in Sec. 3.3 we analyse a smooth version of the phase sequence. From it, we concluded that smooth versions produce similar robustness for the quantum-state exchange.

In Chapter 4 we studied the dynamics for strong and weak coupling regimes of the optomechanical system. We showed that those regimes can be seen as the well-known \mathcal{PT} -symmetric regimes, Sec. 4.1.1. It is remarkable to say that such type of phenomenon is possible because the optomechanical system has losses, without them the only possible behaviour is the quantum-state swap. Then, we proposed the laser's power as control parameter to reveal the characteristic behaviours corresponding to each \mathcal{PT} -symmetric regime. We used two approaches for the analysis, a non-Hermitian Hamiltonian derived from the quantum Langevin


equations and the Lindblad master equation, Sec. 4.2. To present the numerical evolutions, we found useful to introduce the instantaneous renormalized numbers. Even though the resultant evolutions show differences, these quantities exhibit the expected behaviours corresponding to each \mathcal{PT} -symmetric regime, Sec. 4.2.1. The reason of such differences relies on the nature of the non-Hermitian and Lindblad approaches. The first keeps coherence and provides dissipation without preserving the state norm, while the second preserves the norm of the state and provides dissipation and decoherence. Finally, using analytical expressions derived with the quantum Langevin equations, we studied the time evolution of the system at thermal equilibrium and finite temperature. This is a more realistic scenario for the optomechanical initial quantum states, and the result obtained clearly shows the \mathcal{PT} -symmetric regimes, Fig. 4.4. Probably, this is the most important result because it makes us think that those regimes can be observed and measured in laboratory in an accessible way.

In conclusion, all the results showed in this thesis support our proposed techniques for control in optomechanical systems using just the phase or power of the laser as control parameter. Currently optomechanical experiments could be able to observe and measure the benefits and phenomena reported in Chapters 3 and 4. Additionally, we just developed analysis for the red-detuned case, but it seems possible to translate these techniques to the blue-detuned case. Further and more detailed analysis must be done because it is there where the optomechanical bistability occurs, Sec. 2.1.2.

Appendix A

Publications derived from the
research presented in this thesis

SCIENTIFIC REPORTS



OPEN

Robust optomechanical state transfer under composite phase driving

C. Ventura-Velázquez¹, Benjamín Jaramillo Ávila², Elica Kyoseva^{3,4} & B. M. Rodríguez-Lara^{1,5}

We propose a technique for robust optomechanical state transfer using phase-tailored composite pulse driving with constant amplitude. Our proposal is inspired by coherent control techniques in lossless driven qubits. We demonstrate that there exist optimal phases for maximally robust excitation exchange in lossy strongly-driven optomechanical state transfer. In addition, our proposed composite phase driving also protects against random variations in the parameters of the system. However, this driving can take the system out of its steady state. For this reason, we use the ideal optimal phases to produce smooth sequences that both maintain the system close to its steady state and optimize the robustness of optomechanical state transfer.

The essence of optomechanical systems (OMS) is the coupling between light and mechanical motion. Advances in micro and nano fabrication techniques have led to optical cavities coupled to micro and nano mechanical oscillators, where the coupling is provided by the radiation pressure of photons in the optical cavity acting over the mechanical elements. These optical cavities are typically pumped by a laser, which serves as a tool to control the system. Cavity optomechanical systems evolved from the Fabry-Pérot cavity to a plethora of devices like microtoroids and microresonators¹, photonic crystals², superconducting microwave circuits^{3,4}, ultracold atoms⁵, among many others^{6–8}.

Optomechanical systems display a range of physical effects that make them a powerful platform for high-precision metrology and quantum-state control. They show bistable behavior⁹, which is equivalent to that of a Kerr medium¹⁰, and display selective transfer over narrow wavelength windows, known as optomechanically-induced transparency^{11,12}. The latter is equivalent to electromagnetically induced transparency in atoms^{13–15} and its plasmonic and metamaterial analogs^{16–18}. In cavity optomechanical systems, the motion of the mechanical oscillator can be cooled by tuning the laser that pumps the cavity^{19–22}, leading to experiments where a nano-oscillator is cooled to its quantum-mechanical ground state^{23–25}. Previous works propose diverse techniques to enhance optomechanical cooling, for example, by dynamically modifying the damping²⁶, using squeezed light^{27–30}, feedback-controlled light^{31,32}, or considering the effects of non-Markovian evolution³³. These developments show that optomechanical effects allow control over quantum optical and mechanical states leading to exciting proposals to use these systems as transducers^{34–39}.

In the following, we review the formalism that describes quantum excitation exchange in strongly-driven optomechanical systems. The result is a well-known linearized lossy model. Next, we draw from lossless coherent control techniques in qubits^{40,41} and extend them to this linearized effective model of optomechanical systems. Our proposal relies on constant-amplitude composite phase-dependent pumping to achieve robust optomechanical state transfer. This phase-dependent driving produces interference in the evolution of cavity and mechanical quantum states. We engineer this interference to minimize the effect of deviations in the parameters that characterize the system, *i.e.* to produce robust optomechanical state transfer. For the sake of completeness, we produce a central-limit analysis allowing for random variations in the physical parameters that characterize the optomechanical system and compare results from the standard constant-phase sideband state transfer and our method. Next, we discuss the effects of composite phase sequences on the semiclassical steady-state of an optomechanical

¹Instituto Nacional de Astrofísica, Óptica y Electrónica, Calle Luis Enrique Erro No. 1. Sta. Ma. Tonantzintla, Pue. C.P., 72840, Mexico. ²CONACYT-Instituto Nacional de Astrofísica, Óptica y Electrónica, Calle Luis Enrique Erro No. 1. Sta. Ma. Tonantzintla, Pue. C.P., 72840, Mexico. ³Institute of Solid State Physics, Bulgarian Academy of Sciences, 72 Tsarigradsko Chaussée, 1784, Sofia, Bulgaria. ⁴Condensed Matter Physics Department, School of Physics and Astronomy, Tel Aviv University, Tel Aviv, 69978, Israel. ⁵Tecnologico de Monterrey, Escuela de Ingeniería y Ciencias, Ave. Eugenio Garza Sada 2501, Monterrey, N.L., 64849, Mexico. Correspondence and requests for materials should be addressed to B.J.A. (email: jaramillo@inaoep.mx)

\mathcal{PT} -symmetry from Lindblad dynamics in an optomechanical system

B. Jaramillo Ávila,¹ C. Ventura-Velázquez,² R. de J.

León-Montiel,³ Y. N. Joglekar,⁴ and B. M. Rodríguez-Lara^{5,2}

¹*CONACYT-Instituto Nacional de Astrofísica, Óptica y Electrónica,
Calle Luis Enrique Erro No. 1. Sta. Ma. Tonantzintla, Pue. C.P. 72840, México.*

²*Instituto Nacional de Astrofísica, Óptica y Electrónica,
Calle Luis Enrique Erro No. 1. Sta. Ma. Tonantzintla, Pue. C.P. 72840, México.*

³*Instituto de Ciencias Nucleares, Universidad Nacional Autónoma de México,
Apartado Postal 70-543, 04510 Cd. Mx., México.*

⁴*Department of Physics, Indiana University Purdue University
Indianapolis (IUPUI), Indianapolis, Indiana 46202 USA.*

⁵*Tecnologico de Monterrey, Escuela de Ingeniería y Ciencias,
Ave. Eugenio Garza Sada 2501, Monterrey, N.L., México, 64849.*

(Dated: August 12, 2019)

Abstract

The optomechanical state transfer protocol provides effective, lossy, quantum beam-splitter-like dynamics where the strength of the coupling between the electromagnetic and mechanical modes is controlled by the optical steady-state amplitude. By restricting to a subspace with no losses, we argue that the transition from mode-hybridization in the strong coupling regime to the damped-dynamics in the weak coupling regime, is a signature of the passive parity-time (\mathcal{PT}) symmetry breaking transition in the underlying non-Hermitian quantum dimer. We compare the dynamics generated by the quantum open system (Langevin or Lindblad) approach to that of the \mathcal{PT} -symmetric Hamiltonian, to characterize the cases where the two are identical. Additionally, we numerically explore the evolution of separable and correlated number states at zero temperature as well as thermal initial state evolution at room temperature. Our results provide a pathway for realizing non-Hermitian Hamiltonians in optomechanical systems at a quantum level.

Bibliography

- [1] M. Aspelmeyer, T. J. Kippenberg, and F. Marquardt, “Cavity optomechanics,” *Rev. Mod. Phys.*, vol. 86, pp. 1391–1452, 2014.
- [2] T. Kippenberg and K. Vahala, “Cavity opto-mechanics,” *Opt. Express*, vol. 15, no. 25, pp. 17172–17205, 2007.
- [3] J. H. Poynting, *The Pressure of Light. The Romance of Science*, New York: E. S. Gorham, 1910.
- [4] J. C. Maxwell, *A treatise on electricity and magnetism*, vol. 1,2. Oxford: Clarendon Press, 1873.
- [5] E. F. Nichols and G. F. Hull, “A preliminary communication on the pressure of heat and light radiation,” *Phys. Rev. (Series I)*, vol. 13, no. 5, pp. 307–320, 1901.
- [6] P. N. Lebedev, “Experimental examination of light pressure,” *Ann. der Physik*, vol. 311, no. 11, pp. 433–458, 1901.
- [7] E. F. Nichols and G. F. Hull, “The pressure due to radiation. (second paper),” *Phys. Rev. (Series I)*, vol. 17, pp. 26–50, 1903.
- [8] R. A. Beth, “Mechanical detection and measurement of the angular momentum of light,” *Phys. Rev.*, vol. 50, pp. 115–127, 1936.
- [9] D. M. Miles J. Padgett, Justin E. Molloy, ed., *Optical tweezers: methods and applications*. Series in optics and optoelectronics, Taylor and Francis Group, 2010.
- [10] A. Ashkin, “Acceleration and trapping of particles by radiation pressure,” *Phys. Rev. Lett.*, vol. 24, no. 4, pp. 156–159, 1970.
- [11] A. Ashkin and J. M. Dziedzic, “Optical levitation by radiation pressure,” *Appl. Phys. Lett.*, vol. 19, no. 8, pp. 283–385, 1971.
- [12] A. Ashkin, J. M. Dziedzic, J. E. Bjorkholm, and S. Chu, “Observation of a single-beam gradient force optical trap for dielectric particles,” *Opt. Lett.*, vol. 11, no. 5, pp. 288–290, 1986.
- [13] Q. Lin, J. Rosenberg, X. Jiang, K. J. Vahala, and O. Painter, “Mechanical oscillation and cooling actuated by the optical gradient force,” *Phys. Rev. Lett.*, vol. 103, p. 103601, 2009.

-
- [14] D. V. Thourhout and J. Roels, “Optomechanical device actuation through the optical gradient force,” *Nature Photonics*, vol. 4, pp. 211–217, 2010.
- [15] V. B. Braginskiĭ and A. B. Manukin, “Ponderomotive effects of electromagnetic radiation,” *Sov. Phys. JETP*, vol. 25, no. 4, pp. 653–655, 1967.
- [16] V. B. Braginskiĭ, “Classical and quantum restrictions on the detection of weak disturbances of a macroscopic oscillator,” *Sov. Phys. JETP*, vol. 26, no. 4, pp. 831–834, 1968.
- [17] V. B. Braginskiĭ and V. S. Nazarenko, “Quantum properties of a macroscopic oscillator,” *Sov. Phys. JETP*, vol. 30, no. 4, pp. 770–771, 1970.
- [18] V. B. Braginskiĭ, A. B. Manukin, and M. Y. Tikhonov, “Investigation of dissipative ponderomotive effects of electromagnetic radiation,” *Sov. Phys. JETP*, vol. 31, no. 5, pp. 829–830, 1970.
- [19] V. B. Braginskiĭ and Y. I. Vorontsov, “Quantum-mechanical limitations in macroscopic experiments and modern experimental technique,” *Soviet Physics Uspekhi*, vol. 17, no. 5, pp. 644–650, 1975.
- [20] A. Dorsel, J. D. McCullen, P. Meystre, E. Vignes, and H. Walther, “Optical bistability and mirror confinement induced by radiation pressure,” *Phys. Rev. Lett.*, vol. 51, no. 17, pp. 1550–1553, 1983.
- [21] A. Gozzini, I. Longo, S. Barbarino, F. Maccarrone, and F. Mango, “Light-pressure bistability at microwave frequencies,” *J. Opt. Soc. Am. B*, vol. 2, no. 11, pp. 1841–1845, 1985.
- [22] P. Meystre, J. D. McCullen, E. Vignes, and E. M. Wright, “Theory of radiation-pressure-driven interferometers,” *J. Opt. Soc. Am. B*, vol. 2, no. 11, pp. 1830–1840, 1985.
- [23] L. Hilico, J. M. Courty, C. Fabre, E. Giacobino, I. Abram, and J. L. Oudar, “Squeezing with $\chi(3)$ materials,” *Applied Physics B*, vol. 55, no. 3, pp. 202–209, 1992.
- [24] S. Aldana, C. Bruder, and A. Nunnenkamp, “Equivalence between an optomechanical system and a kerr medium,” *Phys. Rev. A*, vol. 88, p. 043826, 2013.
- [25] C. Fabre, M. Pinard, S. Bourzeix, A. Heidmann, E. Giacobino, and S. Reynaud, “Quantum-noise reduction using a cavity with a movable mirror,” *Phys. Rev. A*, vol. 49, pp. 1337–1343, 1994.
- [26] S. Mancini and P. Tombesi, “Quantum noise reduction by radiation pressure,” *Phys. Rev. A*, vol. 49, pp. 4055–4065, 1994.
- [27] K. Jacobs, P. Tombesi, M. J. Collett, and D. F. Walls, “Quantum-nondemolition measurement of photon number using radiation pressure,” *Phys. Rev. A*, vol. 49, pp. 1961–1966, 1994.

- [28] M. Pinard, C. Fabre, and A. Heidmann, “Quantum-nondemolition measurement of light by a piezoelectric crystal,” *Phys. Rev. A*, vol. 51, pp. 2443–2449, 1995.
- [29] S. Mancini, D. Vitali, and P. Tombesi, “Optomechanical cooling of a macroscopic oscillator by homodyne feedback,” *Phys. Rev. Lett.*, vol. 80, pp. 688–691, 1998.
- [30] S. Mancini, V. I. Man’ko, and P. Tombesi, “Ponderomotive control of quantum macroscopic coherence,” *Phys. Rev. A*, vol. 55, pp. 3042–3050, 1997.
- [31] S. Bose, K. Jacobs, and P. L. Knight, “Preparation of nonclassical states in cavities with a moving mirror,” *Phys. Rev. A*, vol. 56, pp. 4175–4186, 1997.
- [32] W. Marshall, C. Simon, R. Penrose, and D. Bouwmeester, “Towards quantum superpositions of a mirror,” *Phys. Rev. Lett.*, vol. 91, p. 130401, 2003.
- [33] J. Zhang, K. Peng, and S. L. Braunstein, “Quantum-state transfer from light to macroscopic oscillators,” *Phys. Rev. A*, vol. 68, p. 013808, 2003.
- [34] M. Hafezi and P. Rabl, “Optomechanically induced non-reciprocity in microring resonators,” *Opt. Express*, vol. 20, no. 7, pp. 7672–7684, 2012.
- [35] P. Rabl, “Photon blockade effect in optomechanical systems,” *Phys. Rev. Lett.*, vol. 107, p. 063601, 2011.
- [36] V. Peano, C. Brendel, M. Schmidt, and F. Marquardt, “Topological phases of sound and light,” *Phys. Rev. X*, vol. 5, p. 031011, 2015.
- [37] K. Stannigel, P. Rabl, A. S. Sørensen, M. D. Lukin, and P. Zoller, “Optomechanical transducers for quantum-information processing,” *Phys. Rev. A*, vol. 84, p. 042341, 2011.
- [38] S. Rips, M. Kiffner, I. Wilson-Rae, and M. J. Hartmann, “Steady-state negative wigner functions of nonlinear nanomechanical oscillators,” *New J. Phys.*, vol. 14, no. 2, p. 023042, 2012.
- [39] J. Restrepo, C. Ciuti, and I. Favero, “Single-polariton optomechanics,” *Phys. Rev. Lett.*, vol. 112, p. 013601, 2014.
- [40] M. Schmidt, V. Peano, and F. Marquardt, “Optomechanical dirac physics,” *New J. Phys.*, vol. 17, no. 2, p. 023025, 2015.
- [41] M. Schmidt, S. Kessler, V. Peano, O. Painter, and F. Marquardt, “Optomechanical creation of magnetic fields for photons on a lattice,” *Optica*, vol. 2, no. 7, pp. 635–641, 2015.
- [42] X.-W. Xu, Y.-x. Liu, C.-P. Sun, and Y. Li, “Mechanical \mathcal{PT} symmetry in coupled optomechanical systems,” *Phys. Rev. A*, vol. 92, p. 013852, 2015.

-
- [43] J. Zhang, B. Peng, t. K. Özdemir, Y.-x. Liu, H. Jing, X.-y. Lü, Y.-l. Liu, L. Yang, and F. Nori, “Giant nonlinearity via breaking parity-time symmetry: A route to low-threshold phonon diodes,” *Phys. Rev. B*, vol. 92, p. 115407, 2015.
- [44] S. Barzanjeh, V. Salari, J. A. Tuszynski, M. Cifra, and C. Simon, “Optomechanical proposal for monitoring microtubule mechanical vibrations,” *Phys. Rev. E*, vol. 96, p. 012404, 2017.
- [45] T. Carmon, H. Rokhsari, L. Yang, T. J. Kippenberg, and K. J. Vahala, “Temporal behavior of radiation-pressure-induced vibrations of an optical microcavity phonon mode,” *Phys. Rev. Lett.*, vol. 94, p. 223902, 2005.
- [46] T. J. Kippenberg, H. Rokhsari, T. Carmon, A. Scherer, and K. J. Vahala, “Analysis of radiation-pressure induced mechanical oscillation of an optical microcavity,” *Phys. Rev. Lett.*, vol. 95, p. 033901, 2005.
- [47] A. Schliesser, P. Del’Haye, N. Nooshi, K. J. Vahala, and T. J. Kippenberg, “Radiation pressure cooling of a micromechanical oscillator using dynamical backaction,” *Phys. Rev. Lett.*, vol. 97, p. 243905, 2006.
- [48] O. Arcizet, P. F. Cohadon, T. Briant, M. Pinard, and A. Heidmann, “Radiation-pressure cooling and optomechanical instability of a micromirror,” *Nature*, vol. 444, pp. 71–74, 2006.
- [49] S. Gigan, H. R. Böhm, M. Paternostro, F. Blaser, G. Langer, J. B. Hertzberg, K. C. Schwab, D. Buerle, M. Aspelmeyer, and A. Zeilinger, “Self-cooling of a micromirror by radiation pressure,” *Nature*, vol. 444, pp. 67–70, 2006.
- [50] J. D. Thompson, B. M. Zwickl, A. M. Jayich, F. Marquardt, S. M. Girvin, and J. G. E. Harris, “Strong dispersive coupling of a high-finesse cavity to a micromechanical membrane,” *Nature*, vol. 452, pp. 72–75, 2008.
- [51] D. J. Wilson, C. A. Regal, S. B. Papp, and H. J. Kimble, “Cavity optomechanics with stoichiometric thin films,” *Phys. Rev. Lett.*, vol. 103, p. 207204, 2009.
- [52] X. Jiang, Q. Lin, J. Rosenberg, K. Vahala, and O. Painter, “High-q double-disk microcavities for cavity optomechanics,” *Opt. Express*, vol. 17, no. 23, pp. 20911–20919, 2009.
- [53] G. S. Wiederhecker, L. Chen, A. Gondarenko, and M. Lipson, “Controlling photonic structures using optical forces,” *Nature*, vol. 462, pp. 633–636, 2009.
- [54] R. Ma, A. Schliesser, P. Del’Haye, A. Dabirian, G. Anetsberger, and T. J. Kippenberg, “Radiation-pressure-driven vibrational modes in ultrahigh-q silica microspheres,” *Opt. Lett.*, vol. 32, no. 15, pp. 2200–2202, 2007.
- [55] Y.-S. Park and H. Wang, “Resolved-sideband and cryogenic cooling of an optomechanical resonator,” *Nature Physics*, vol. 5, pp. 489–493, 2009.

- [56] M. Tomes and T. Carmon, “Photonic micro-electromechanical systems vibrating at x -band (11-ghz) rates,” *Phys. Rev. Lett.*, vol. 102, p. 113601, 2009.
- [57] M. Eichenfield, R. Camacho, J. Chan, K. J. Vahala, and O. Painter, “A picogram- and nanometre-scale photonic-crystal optomechanical cavity,” *Nature*, vol. 49, pp. 550–555, 2009.
- [58] M. Eichenfield, J. Chan, R. M. Camacho, K. J. Vahala, and O. Painter, “Optomechanical crystals,” *Nature*, vol. 462, pp. 78–82, 2009.
- [59] J. D. Teufel, J. W. Harlow, C. A. Regal, and K. W. Lehnert, “Dynamical backaction of microwave fields on a nanomechanical oscillator,” *Phys. Rev. Lett.*, vol. 101, p. 197203, 2008.
- [60] G. Anetsberger, O. Arcizet, Q. P. Unterreithmeier, R. Rivière, A. Schliesser, E. M. Weig, J. P. Kotthaus, and T. J. Kippenberg, “Near-field cavity optomechanics with nanomechanical oscillators,” *Nature Physics*, vol. 5, pp. 909–914, 2009.
- [61] C. Eichler and J. R. Petta, “Realizing a circuit analog of an optomechanical system with longitudinally coupled superconducting resonators,” *Phys. Rev. Lett.*, vol. 120, p. 227702, 2018.
- [62] N. Kiesel, F. Blaser, U. Deli c, D. Grass, R. Kaltenbaek, and M. Aspelmeyer, “Cavity cooling of an optically levitated submicron particle,” *Proceedings of the National Academy of Sciences*, vol. 110, no. 35, pp. 14180–14185, 2013.
- [63] F. Brennecke, S. Ritter, T. Donner, and T. Esslinger, “Cavity optomechanics with a bose-einstein condensate,” *Science*, vol. 322, no. 5899, pp. 235–238, 2008.
- [64] K. W. Murch, K. L. Moore, S. Gupta, and D. M. Stamper-Kurn, “Observation of quantum-measurement backaction with an ultracold atomic gas,” *Nat. Phys.*, vol. 4, pp. 561–564, 2008.
- [65] K. H. Kim, G. Bahl, W. Lee, J. Liu, M. Tomes, X. Fan, and T. Carmon, “Cavity optomechanics on a microfluidic resonator with water and viscous liquids,” *Light: Sci. Appl.*, vol. 3, no. e110, 2013.
- [66] R. Dahan, L. L. Martin, and T. Carmon, “Droplet optomechanics,” *Optica*, vol. 3, no. 2, pp. 175–178, 2016.
- [67] A. D. Kashkanova, A. B. Shkarin, C. D. Brown, N. E. Flowers-Jacobs, L. Childress, S. W. Hoch, L. Hohmann, K. Ott, J. Reichel, and J. G. E. Harris, “Superfluid brillouin optomechanics,” *Nature Physics*, vol. 13, pp. 74–79, 2017.
- [68] A. D. Kashkanova, A. B. Shkarin, C. D. Brown, N. E. Flowers-Jacobs, L. Childress, S. W. Hoch, L. Hohmann, K. Ott, J. Reichel, and J. G. E. Harris, “Optomechanics in superfluid helium coupled to a fiber-based cavity,” *Journal of Optics*, vol. 19, no. 3, p. 034001, 2017.

-
- [69] J. Chan, T. P. M. Alegre, A. H. Safavi-Naeini, A. K. Jeff T. Hill, S. Gröblacher, M. Aspelmeyer, and O. Painter, “Laser cooling of a nanomechanical oscillator into its quantum ground state,” *Nature*, vol. 478, pp. 89–92, 2011.
- [70] J. D. Teufel, T. Donner, D. Li, J. W. Harlow, M. S. Allman, K. Cicak, A. J. Sirois, J. D. Whittaker, K. W. Lehnert, and R. W. Simmonds, “Sideband cooling of micromechanical motion to the quantum ground state,” *Nature*, vol. 475, pp. 359–363, 2011.
- [71] R. Rivière, S. Deléglise, S. Weis, E. Gavartin, O. Arcizet, A. Schliesser, and T. J. Kippenberg, “Optomechanical sideband cooling of a micromechanical oscillator close to the quantum ground state,” *Phys. Rev. A*, vol. 83, p. 063835, 2011.
- [72] S. Weis, R. Rivière, S. Deléglise, E. Gavartin, O. Arcizet, A. Schliesser, and T. J. Kippenberg, “Optomechanically induced transparency,” *Science*, vol. 330, no. 6010, pp. 1520–1523, 2010.
- [73] A. H. Safavi-Naeini, T. P. M. Alegre, J. Chan, M. Eichenfield, M. Winger, Q. Lin, J. T. Hill, D. E. Chang, and O. Painter, “Electromagnetically induced transparency and slow light with optomechanics,” *Nature*, vol. 472, pp. 69–73, 2011.
- [74] M. Karuza, C. Biancofiore, M. Bawaj, C. Molinelli, M. Galassi, R. Natali, P. Tombesi, G. Di Giuseppe, and D. Vitali, “Optomechanically induced transparency in a membrane-in-the-middle setup at room temperature,” *Phys. Rev. A*, vol. 88, p. 013804, 2013.
- [75] S. Gröblacher, K. Hammerer, M. R. Vanner, and M. Aspelmeyer, “Observation of strong coupling between a micromechanical resonator and a optical cavity field,” *Nature*, vol. 460, pp. 724–727, 2009.
- [76] T. A. Palomaki, J. D. Teufel, R. W. Simmonds, and K. W. Lehnert, “Entangling mechanical motion with microwave fields,” *Science*, vol. 342, pp. 710–713, 2013.
- [77] R. Riedinger, A. Wallucks, I. Marinković, C. Löschnauer, M. Aspelmeyer, S. Hong, and S. Gröblacher, “Remote quantum entanglement between two micromechanical oscillators,” *Nature*, vol. 556, pp. 473–477, 2018.
- [78] C. F. Ockeloen-Korppi, E. Damskög, J.-M. Pirkkalainen, M. Asjad, A. A. Clerk, F. Massel, M. J. Woolley, and M. A. Sillanp, “Stabilized entanglement of massive mechanical oscillators,” *Nature*, vol. 556, pp. 478–482, 2018.
- [79] F. Lecocq, J. D. Teufel, J. Aumentado, and R. W. Simmonds, “Resolving the vacuum fluctuations of an optomechanical system using an artificial atom,” *Nature Physics*, vol. 11, pp. 635–639, 2015.
- [80] E. E. Wollman, C. U. Lei, A. J. Weinstein, J. Suh, A. Kronwald, F. Marquardt, A. A. Clerk, and K. C. Schwab, “Quantum squeezing of motion in a mechanical resonator,” *Science*, 2015.

- [81] N. R. Bernier, L. D. Tóth, A. Koottandavida, M. A. Ioannou, D. Malz, A. Nunnenkamp, A. K. Feofanov, and T. J. Kippenberg, “Nonreciprocal reconfigurable microwave optomechanical circuit,” *Nat. Commun.*, vol. 8, no. 604, 2017.
- [82] S. Barzanjeh, M. Wulf, M. Peruzzo, M. Kalaei, P. Dieterle, O. Painter, and J. Fink, “Mechanical on-chip microwave circulator,” *Nature Communications*, vol. 8, no. 953, 2017.
- [83] R. Riedinger, S. Hong, R. A. Norte, J. A. Slater, J. Shang, e. Alexander G. Kraus, V. Anant, M. Aspelmeyer, and S. Gröblacher, “Non-classical correlations between single photons and phonons from a mechanical oscillator,” *Nature*, vol. 530, pp. 313–316, 2016.
- [84] S. Hong, R. Riedinger, I. Marinković, A. Wallucks, S. G. Hofer, R. A. Norte, M. Aspelmeyer, and S. Gröblacher, “Hanbury brown and twiss interferometry of single phonons from an optomechanical resonator,” *Science*, vol. 358, no. 6360, pp. 203–206, 2017.
- [85] I. Marinković, A. Wallucks, R. Riedinger, S. Hong, M. Aspelmeyer, and S. Gröblacher, “Optomechanical bell test,” *Phys. Rev. Lett.*, vol. 121, p. 220404, 2018.
- [86] E. Verhagen, S. Deléglise, a. S. S. Weis, and T. J. Kippenberg, “Quantum-coherent coupling of a mechanical oscillator to an optical cavity mode,” *Nature*, vol. 482, pp. 63–67, 2012.
- [87] A. F. Pace, M. J. Collett, and D. F. Walls, “Quantum limits in interferometric detection of gravitational radiation,” *Phys. Rev. A*, vol. 47, pp. 3173–3189, 1993.
- [88] C. K. Law, “Interaction between a moving mirror and radiation pressure: A hamiltonian formulation,” *Phys. Rev. A*, vol. 51, pp. 2537–2541, 1995.
- [89] J. C. Sankey, C. Yang, B. M. Zwickl, A. M. Jayich, and J. G. E. Harris, “Strong and tunable nonlinear optomechanical coupling in low-loss system,” *Nat. Phys.*, vol. 6, pp. 707 – 712, 2010.
- [90] T. Rocheleau, T. Ndukum, C. Macklin, J. B. Hertzberg, A. A. Clerk, and K. C. Schwab, “Preparation and detection of a mechanical resonator near the ground state of motion,” *Nature*, vol. 463, pp. 72–75, 2010.
- [91] A. A. Gangat, T. M. Stace, and G. J. Milburn, “Phonon number quantum jumps in an optomechanical system,” *New Journal of Physics*, vol. 13, no. 4, p. 043024, 2011.
- [92] D. Walls and G. J. Milburn, *Quantum Optics*. Springer-Verlag Berlin Heidelberg, 2 ed., 2008.
- [93] A. Nunnenkamp, K. Børkje, and S. M. Girvin, “Single-photon optomechanics,” *Phys. Rev. Lett.*, vol. 107, p. 063602, 2011.
- [94] C. Ventura-Velázquez, B. M. Rodríguez-Lara, and H. M. Moya-Cessa, “Operator approach to quantum optomechanics,” *Phys. Scr.*, vol. 90, no. 6, p. 068010, 2015.

-
- [95] F. Marquardt, J. G. E. Harris, and S. M. Girvin, “Dynamical multistability induced by radiation pressure in high-finesse micromechanical optical cavities,” *Phys. Rev. Lett.*, vol. 96, p. 103901, 2006.
- [96] S. Haroche and J.-M. Raimond, *Exploring the Quantum: Atoms, Cavities, and Photons*. Oxford University Press, 1st ed., 2006.
- [97] J. D. Cohen, S. M. Meenehan, G. S. MacCabe, S. Gröblacher, A. H. Safavi-Naeini, F. Marsili, M. D. Shaw, and O. Painter, “Phonon counting and intensity interferometry of a nanomechanical resonator,” *Nature*, vol. 520, pp. 522–525, 2015.
- [98] S. Gröblacher, A. Trubarov, N. Prigge, G. D. Cole, M. Aspelmeyer, and J. Eisert, “Observation of non-markovian micromechanical brownian motion,” *Nat. Commun.*, vol. 6, no. 7606, 2015.
- [99] R. Schilling, H. Schütz, A. H. Ghadimi, V. Sudhir, D. J. Wilson, and T. J. Kippenberg, “Near-field integration of a sin nanobeam and a sio₂ microcavity for heisenberg-limited displacement sensing,” *Phys. Rev. Applied*, vol. 5, p. 054019, 2016.
- [100] B. T. Torosov and N. V. Vitanov, “Smooth composite pulses for high-fidelity quantum information processing,” *Phys. Rev. A*, vol. 83, p. 053420, 2011.
- [101] B. T. Torosov, S. Guérin, and N. V. Vitanov, “High-fidelity adiabatic passage by composite sequences of chirped pulses,” *Phys Rev Lett*, vol. 106, p. 233001, 2011.
- [102] E. Kyoseva and N. V. Vitanov, “Arbitrarily accurate passband composite pulses for dynamical suppression of amplitude noise,” *Phys. Rev. A*, vol. 88, p. 063410, 2013.
- [103] B. T. Torosov and N. V. Vitanov, “High-fidelity error-resilient composite phase gates,” *Phys. Rev. A*, vol. 90, p. 012341, 2014.
- [104] D. Schraft, T. Halfmann, G. T. Genov, and N. V. Vitanov, “Experimental demonstration of composite adiabatic passage,” *Phys. Rev. A*, vol. 88, p. 063406, 2013.
- [105] C. W. Gardiner and M. J. Collett, “Input and output in damped quantum systems: Quantum stochastic differential equations and the master equation,” *Phys. Rev. A*, vol. 31, pp. 3761–3774, 1985.
- [106] C. W. Gardiner and P. Zoller, *Quantum Noise, A Handbook of Markovian and Non-Markovian Quantum Stochastic Methods with Applications to Quantum Optics*. Springer Series in Synergetics, Springer-Verlag Berlin Heidelberg, 3rd ed., 2004.
- [107] R. Tycko, “Broadband population inversion,” *Phys. Rev. Lett.*, vol. 51, pp. 775–777, 1983.
- [108] M. A. Nielsen and I. L. Chuang, *Quantum Computation and Quantum Information*. Cambridge University Press, 1st ed., 2010.
- [109] N. Zettili, *Quantum Mechanics, Concepts and Applications*. John Wiley & Sons, Ltd, 2nd ed., 2009.

- [110] C. M. Bender and S. Boettcher, “Real spectra in non-hermitian hamiltonians having \mathcal{PT} symmetry,” *Phys. Rev. Lett.*, vol. 80, pp. 5243–5246, 1998.
- [111] C. M. Bender, “Making sense of non-hermitian hamiltonians,” *Rep. Prog. Phys.*, vol. 70, no. 6, pp. 947–1018, 2007.
- [112] A. Ruschhaupt, F. Delgado, and J. G. Muga, “Physical realization of \mathcal{PT} -symmetric potential scattering in a planar slab waveguide,” *J. Phys. A: Math. Gen.*, vol. 38, no. 9, pp. L171–L176, 2005.
- [113] R. El-Ganainy, K. G. Makris, D. N. Christodoulides, and Z. H. Musslimani, “Theory of coupled optical \mathcal{PT} -symmetric structures,” *Opt. Lett.*, vol. 32, no. 17, pp. 2632–2634, 2007.
- [114] J. D. Huerta Morales, J. Guerrero, S. Lpez-Aguayo, and B. M. Rodríguez-Lara, “Revisiting the optical \mathcal{PT} -symmetric dimer,” *Symmetry*, vol. 8, no. 9, 2016.
- [115] A. Guo, G. J. Salamo, D. Duchesne, R. Morandotti, M. Volatier-Ravat, V. Aimez, G. A. Siviloglou, and D. N. Christodoulides, “Observation of \mathcal{PT} -symmetry breaking in complex optical potentials,” *Phys. Rev. Lett.*, vol. 103, p. 093902, 2009.
- [116] N. Moiseyev and S. Friedland, “Association of resonance states with the incomplete spectrum of finite complex-scaled hamiltonian matrices,” *Phys. Rev. A*, vol. 22, pp. 618–624, 1980.
- [117] B. M. Rodríguez-Lara and J. Guerrero, “Optical finite representation of the lorentz group,” *Opt. Lett.*, vol. 40, no. 23, pp. 5682–5685, 2015.
- [118] J. J. Sakurai, *Modern Quantum Mechanics*. Addison-Wesley Publishing Company, 1994.
- [119] C. Ventura-Velázquez, B. J. Ávila, E. Kyoseva, and B. M. Rodríguez-Lara, “Robust optomechanical state transfer under composite phase driving,” *Sci. Rep.*, vol. 9, no. 4382, 2019.
- [120] F. Marquardt, J. P. Chen, A. A. Clerk, and S. M. Girvin, “Quantum theory of cavity-assisted sideband cooling of mechanical motion,” *Phys. Rev. Lett.*, vol. 99, p. 093902, 2007.
- [121] J. M. Dobrindt, I. Wilson-Rae, and T. J. Kippenberg, “Parametric normal-mode splitting in cavity optomechanics,” *Phys. Rev. Lett.*, vol. 101, p. 263602, 2008.